

Manuscript prepared for Geosci. Model Dev.
with version 2014/09/16 7.15 Copernicus papers of the L^AT_EX class copernicus.cls.
Date: 20 August 2015

Addressing the Challenge of Nonphysical Solution Negativity in Coupling a Reactive Transport Code with a Global Land Surface Model for Mechanistic Biogeochemistry Representation

Guoping Tang¹, Fengming Yuan¹, Gautam Bisht^{1,2}, Glenn E. Hammond³, Peter C. Lichtner⁴, Jitendra Kumar¹, Richard T. Mills^{1,5}, Xiaofeng Xu^{1,6}, Ben Andre⁷, Forrest M. Hoffman¹, Scott L. Painter¹, and Peter E. Thornton¹

¹Oak Ridge National Laboratory, Oak Ridge, Tennessee, United States

²Lawrence Berkeley National Laboratory, Berkeley, California, United States

³Sandia National Laboratories, Albuquerque, New Mexico, United States

⁴OFM Research, Redmond, Washington, United States

⁵Intel Incorporation, Portland, Oregon, United States

⁶University of Texas at El Paso, El Paso, Texas, United States

⁷National Center for Atmospheric Research, Boulder, Colorado, United States

Correspondence to: Peter E. Thornton (thorntonpe@ornl.gov)

This manuscript has been authored by UT-Battelle, LLC under Contract No. DE-AC05-00OR22725 with the U.S. Department of Energy. The United States Government retains and the publisher, by accepting the article for publication, acknowledges that the United States Government retains a non-exclusive, paid-up, irrevocable, world-wide license to publish or reproduce the published form of

- 5 this manuscript, or allow others to do so, for United States Government purposes. The Department of Energy will provide public access to these results of federally sponsored research in accordance with the DOE Public Access Plan(<http://energy.gov/downloads/doe-public-access-plan>).

Abstract. Reactive transport codes (e.g., PFLOTRAN) are increasingly used to improve the representation of biogeochemical processes in terrestrial ecosystem models (e.g., the Community Land Model, CLM). We have developed coupled CLM-PFLOTRAN modeling framework to utilize the reactive transport code PFLOTRAN for flexible and improved representation of biogeochemical processes in CLM. However, as CLM and PFLOTRAN use explicit and implicit time stepping, implementation of CLM biogeochemical reactions in PFLOTRAN can result in negative primary species concentrations, which is not physically meaningful. The objective of this work is to address the nonphysical solution negativity to obtain accurate, efficient, and robust solutions. We illustrate the implementation of a reaction network with the CLM-CN decomposition, nitrification, denitrification, and plant nitrogen uptake reactions and test the implementation at arctic, temperate, and tropical sites. We examine use of scaling back the update during each iteration (SU), log transformation (LT), and downregulating the reaction rate to account for reactant availability limitation to enforce nonnegativity. Both SU and LT guarantee nonnegativity but with implications. When a very small scaling factor occurs due to either consumption or numerical overshoot, and the iterations are deemed converged because of too small an update, SU can introduce excessive numerical error. LT involves multiplication of the Jacobian matrix by the concentration vector, which increases the condition number, decreases the time step size, and increases the computational cost. Neither SU nor LT prevents zero concentration. When the concentration is close to machine precision or 0, a small positive update stops all reactions for SU, and LT can fail due to a singular Jacobian matrix. The consumption rate has to be downregulated such that the solution to the mathematical representation is positive. A first-order rate downregulates consumption and is nonnegative, and adding a residual concentration makes it positive. For zero-order rate or when the reaction rate is not a function of a reactant, representing the availability limitation of each reactant with a Monod substrate limiting function provides a smooth transition between a zero-order rate when the reactant is abundant and first-order rate when the reactant becomes limiting. When the half saturation is small, marching through the transition may require small time step sizes to resolve the sharp change within a small range of concentration values. Our results from simple tests and CLM-PFLOTRAN simulations caution against use of SU and indicate that accurate, stable, and relatively efficient solutions can be achieved with LT and downregulation with Monod substrate limiting function and residual concentration.

1 Introduction

Land surface models calculate the fluxes of energy, water, and green house gases across the land-atmosphere interface for the atmospheric general circulation models for climate simulation and weather forecasting. Evolving from the first generation “bucket”, second generation “biophysical”, and third generation “physiological” models (Sellers et al., 1997; Seneviratne et al., 2010), current land surface models, e.g., the Community Land Model (CLM), implement comprehensive thermal, hydrological, and biogeochemical processes (Oleson et al., 2013). The important role of soil biogeochemistry is suggested by the confirmation that the increase of CO₂, CH₄, and N₂O in the atmosphere since the preindustrial times is the main driving cause of climate change, and inter-dependent water, carbon and nitrogen cycles in terrestrial ecosystems are very sensitive to climate changes (IPCC, 2013). CLM4.5 incorporates CLM-CN and CENTURY, and adds methane models for carbon and nitrogen cycles (Oleson et al., 2013). In addition to ~ 250 soil biogeochemical models developed in the past 80 years (Manzoni and Porporato, 2009), increasingly mechanistic models continue to be developed to increase the fidelity of process representation for improving climate prediction (e.g., Wang et al., 2012; Riley et al., 2014).

As land surface models usually hardcode the reaction network (pools/species, reactions, rate formulae), substantial effort is often required to revise the source code for testing alternative biogeochemical models, and incorporating new process understanding. To mitigate this issue, Fang et al. (2013) demonstrates the use of a reaction-based approach to facilitate implementation of CLM-CN and CENTURY models, and incorporation of phosphorus cycle. While Fang et al. (2013) adds a reaction solver developed from the reactive transport (geochemical) model literature for algebraic and ordinary differential equations, Tang et al. (2013b) solves the advection diffusion equation in CLM using operator splitting with the Crank-Nicolson scheme for diffusion and a forward-in-time upstream discretization for advection. In contrast, a reactive transport code, TOUGH-REACT, is used to develop multi-phase (gas, aqueous, solid) mechanistic carbon and nitrogen cycle models with many speciation and microbial reactions (Maggi et al., 2008; Gu and Riley, 2010; Riley et al., 2014). Coupling a well-developed reactive transport code (e.g., Steefel et al., 2014) with CLM facilitates testing and implementation of increasingly mechanistic biogeochemical models in terrestrial ecosystem models by taking advantages of the developments in reactive transport modeling.

The nonphysical solution negativity arises in the coupling of a reactive transport code with CLM as an essential aspect of these land surface models is the ability to simulate competition for nutrients (e.g., mineral nitrogen, phosphorus, etc.) among plants and microbes. For example, the CLM-CN decomposition cascade downregulates the demand based on the available nitrogen (N) (Oleson et al., 2013; Thornton and Rosenbloom, 2005; ?). Specifically, marching from time step k to $k + 1$ with a supply rate S^k and consumption rate D^k using the forward difference, $[N]^{k+1} = [N]^k + (S^k - D^k)\Delta t$. ($[]$ is used to denote concentration.) CLM replaces D^k with $\min(D^k, [N]^k/\Delta t)$ so that $[N]^{k+1} \geq S^k\Delta t \geq 0$. As a result, $[N]$ is nonnegative in CLM.

75 Geochemical codes generally use implicit time stepping such as the backward Euler method, $([N]^{k+1} - [N]^k)/\Delta t = S^{k+1} - D^{k+1}$. Solving this nonlinear equation with the Newton-Raphson method to iterate from p to $p + 1$,

$$[N]^{k+1,p+1} = [N]^{k+1,p} - \frac{\frac{[N]^{k+1,p} - [N]^k}{\Delta t} - S^{k+1,p} + D^{k+1,p}}{\frac{1}{\Delta t} - \frac{\partial S^{k+1,p}}{\partial [N]^{k+1,p}} + \frac{\partial D^{k+1,p}}{\partial [N]^{k+1,p}}}. \quad (1)$$

80 Depending on $[N]^k$, Δt , $S^{k+1,p}$, $D^{k+1,p}$, and the derivatives, $[N]^{k+1,p+1}$ can be negative, which is not physical, and can cause numerical instability and errors (Shampine et al., 2005). With instability (divergence), the simulation may abort before reaching target simulation duration. Excess numerical error may jeopardize the improvements in process representation. Avoiding numerical instability and error may result in small time step sizes or high computational cost. Therefore, it is necessary to address the nonphysical solution negativity for accurate, robust, and efficient numerical simulation.

85 Enforcing nonnegativity is a common challenge in science, engineering, and business, including, for example, image processing, optimization, and ecosystem and geochemical modeling (Antonelli et al., 2009; Broekhuizen et al., 2008; Bruggeman et al., 2007; Burchard et al., 2003, 2005; Chen and Plemons, 2009; Pierre and Schmitt, 2000; Shampine et al., 2005). The challenge increases in geochemical modeling because the concentration can be very low. For example, the threshold 90 concentration for H_2 is 1.5 nM (10^{-9} M) for dechlorinators and $5\sim20 \text{ nM}$ for methanogens (Fennell and Gossett, 1998). The EPA maximum contaminant level for drinking water for dioxin is 30 ppq ($3.5 \times 10^{-13} \text{ M}$). The redox potential Eh needs to be decreased to -0.35 V (corresponding to an O_2 concentration $< 10^{-22} \text{ M}$ Hungate, 1975) for methanogens to grow (Jarrell, 1985). With very low concentration, a small consumption or numerical overshoot can lead to negative concentration.

95 Two methods are used to avoid negative concentration in geochemical codes. One is to use the logarithm concentration as the primary variable (Bethke, 2007; Hammond, 2003; Parkhurst and Appelo, 1999). Log transformation (LT) is well suited for solving the mass action equations because it converts these nonlinear equations into linear equations. However, LT converts linear advection and diffusion equations into nonlinear equations, which may increase the computational cost (Hammond, 100 2003). The other approach scales back the update in each of the Newton-Raphson iteration (SU) to enforce nonnegativity (Bethke, 2007; Hammond, 2003). Both methods are available in PFLOTTRAN (Lichtner et al., 2015) and some other geochemical codes (e.g., Geochemist's Workbench, Bethke, 2007). However, to our knowledge, the implications of these approaches have not been thoroughly examined, particularly for application to CLM.

105 Competition for nutrients (for instance, labile carbon, phosphate, O_2 , and H_2) is common in terrestrial ecosystems, and is increasingly incorporated in process-rich models. As the terrestrial ecosystem models are often run under a variety of conditions around the globe for hundreds of years with a time step as small as half an hour, proper treatment of the nonphysical solution negativity is necessary for accurate, efficient, and robust simulation of biogeochemical processes using reactive 110 transport codes for earth system models. The objective of this work is to implement CLM subsur-

face biogeochemical reactions in CLM-PFLOTRAN with the focus on addressing the nonphysical solution negativity to obtain accurate, efficient, and robust solutions. We implement the CLM-CN decomposition (Bonan et al., 2012; Oleson et al., 2013; Thornton and Rosenbloom, 2005); nitrification; denitrification (Dickinson et al., 2002; Parton et al., 2001, 1996); and plant nitrogen uptake reactions
115 in CLM-PFLOTRAN and test the implementation at arctic, temperate, and tropical sites. In addition to SU and LT, we examine ways to downregulate consumption rate to account for the limitation of reactant availability on reaction rate. While this work focuses on addressing the nonphysical solution negativity for biogeochemistry, detailed comparison of the results of CLM and CLM-PFLOTRAN biogeochemistry representation and comprehensive CLM-PFLOTRAN coupling in heat transfer (including freeze and thaw), hydrology, and biogeochemistry will be presented in future publications.
120 While we use CLM-PFLOTRAN to implement and test simple carbon and nitrogen reactions at a few sites, we hope that what we develop here will be relevant for a wide range of applications.

2 CLM-PFLOTRAN biogeochemistry

The terrestrial ecosystem models generally include biogeochemical reactions for carbon and nitrogen cycles, in particular, the organic matter decomposition, nitrification, denitrification and methane production and oxidation. The kinetics are usually described by a first-order rate modified by response functions for environmental variables (temperature, moisture, pH, etc.) (Bonan et al., 2012; Boyer et al., 2006; Schmidt et al., 2011). In this work, we use the CLM-CN decomposition (Bonan et al., 2012; Oleson et al., 2013; Thornton and Rosenbloom, 2005), nitrification, denitrification
130 (Dickinson et al., 2002; Parton et al., 2001, 1996), and plant nitrogen uptake reactions (Fig. 1) as an example. The reactions and rate formulae are detailed in Appendix A.

In CLM-PFLOTRAN, CLM instructs PFLOTRAN to solve the partial differential equations for energy (including freezing and thawing), water flow, and reaction and transport in the surface and subsurface. This work focuses on the biogeochemistry (energy, hydrology and overall coupling will
135 be described in future publications). Specifically, we focus on addressing the nonphysical solution negativity for the geochemical reactions, with CLM solving the energy and water flow equations and handling the solute transport (mixing, advection, diffusion, and leaching).

In each time step, CLM provides production rates for Lit1C, Lit1N, Lit2C, Lit2N, Lit3C, Lit3N for litter fall; CWDC, and CWDN for coarse woody debris production, NH_4^+ and NO_3^- for nitrogen deposition and fixation; and plant N demand (rate); and specifies liquid water content, matrix potential and temperature for PFLOTRAN; PFLOTRAN solves the ordinary differential equations for the kinetic reactions, the mass action equations for the equilibrium equations, and provides the final concentrations back to CLM.

PFLOTRAN does not track individual reaction rates such as total nitrogen mineralization rate. We
145 add optional hypothetical species (diagnostic variables), e.g., PlantN, N_2Od , and DeniN, to track

NO₃⁻ uptake by plants as in reaction (R14); N₂O production from nitrification reaction (R11) due to net mineralization (Eq. A5); and denitrification (R12). At the end of each time step, CLM uses the change of these concentrations to calculate the specific rates. To simplify the calculations, we reset these concentrations to 10⁻¹⁰ at the beginning of each time step instead of storing the values of the
150 previous time step.

The reactions and rates such as those described in Appendix A are implemented using the “reaction sandbox” concept in PFLOTRAN (Lichtner et al., 2015). For each reaction, we specify a rate and a derivative of the rate with respect to any components in the rate formula, given concentrations, temperature, moisture content, grid cell volume, and other environmental variables. PFLOTRAN
155 accumulates these rates and derivatives into a residual vector and a Jacobian matrix, and the global equation is discretized in time using the backward Euler method and solved using the Newton-Raphson method. Ignoring equilibrium reactions and transport for simplicity of discussion in this work, PFLOTRAN solves the ordinary differential equation,

$$\frac{dc}{dt} = \mathbf{R}(c), \quad (2)$$

160 with c as the concentration vector and \mathbf{R} as the kinetic reaction rate. Discretizing Eq. (2) in time using the backward Euler method,

$$\frac{c^{k+1} - c^k}{\Delta t} = \mathbf{R}(c^{k+1}). \quad (3)$$

Solving the equation using the Newton-Raphson method,

$$\mathbf{f}(c^{k+1,p}) = (c^{k+1,p} - c^k)/\Delta t - \mathbf{R}(c^{k+1,p}), \quad (4)$$

165

$$\mathbf{J} = \frac{\partial \mathbf{f}(c^{k+1,p})}{\partial c^{k+1,p}}, \quad (5)$$

$$\delta c^{k+1,p} = \mathbf{J}^{-1} \mathbf{f}(c^{k+1,p}), \quad (6)$$

and

$$170 \quad c^{k+1,p+1} = c^{k+1,p} - \delta c^{k+1,p}. \quad (7)$$

The iteration continues until either the residual $\mathbf{f}(c^{k+1,p})$ or the update $\delta c^{k+1,p}$ is less than a specified tolerance. Specifically,

$$\|\mathbf{f}(c^{k+1,p})\|_2 < \text{ATOL}, \quad (8)$$

$$175 \quad \frac{\|\mathbf{f}(c^{k+1,p})\|_2}{\|\mathbf{f}(c^{k+1,0})\|_2} < \text{RTOL}, \quad (9)$$

$$\frac{\|\delta\mathbf{c}^{k+1,p}\|_2}{\|\mathbf{c}^{k+1,p}\|_2} < \text{STOL}, \quad (10)$$

$$\|\mathbf{f}(\mathbf{c}^{k+1,p})\|_\infty < \text{ITOL_RES}, \quad (11)$$

180 or

$$\|\delta\mathbf{c}^{k+1,p}\|_\infty < \text{ITOL_UPDATE}. \quad (12)$$

If none of these tolerances are met in MAXIT iterations or MAXF function evaluations, the iteration is considered to diverge, and PFLOTRAN decreases the time step size for MAX_CUT times. The default values in PFLOTRAN are ATOL = 10^{-50} , RTOL = 10^{-8} , STOL = 10^{-8} , ITOL_RES = 185 10^{-50} , ITOL_UPDATE = 10^{-50} , MAXIT = 50, MAXF = 10^4 , and MAX_CUT = 16.

Unlike the explicit time stepping in CLM for biogeochemistry where only the reaction rates need to be calculated, the implicit time stepping used in PFLOTRAN and other geochemical codes requires the derivatives. While PFLOTRAN provides the option to calculate the derivatives numerically, analytical derivative calculation is generally preferred (e.g., Xu et al., 2006) because numerical calculation for accurate Jacobian approximation is a notoriously difficult task (Shampine et al., 2005).

Many reactions can be specified, and the rates and derivatives are accumulated in the residual and Jacobian, providing flexibility in specifying various reactions with a user-defined rate formula. As typical rate formulae consist of first order, Monod, and/or inhibition terms, a general rate formula 195 with flexible number of terms and typical moisture, temperature, and pH response functions are coded in PFLOTRAN. Most of the biogeochemical reactions can be specified in the input file, with flexible number of reactions, pools (species), rate terms, and various response functions without source code modification. Code modification is necessary only when different rate formulae, or response functions are introduced. In contrast, the number of pools and reactions are traditionally 200 hard-coded in CLM. Consequently, any change of the pools, reactions, or rage formula requires source code modification. Therefore, this new approach facilitates implementation of increasingly mechanistic reactions and tests of various representations with reduced code modifications.

3 Approaches for addressing the nonphysical solution negativity

Like Eq. (1), one of the basic challenges for using a numerical geochemical formulation for CLM is 205 that the updated solution in Eq. (7) is not guaranteed to be nonnegative. Both SU (scaling back the update during each iteration) and LT (log transformation) are available in PFLOTRAN to enforce nonnegativity. However, to our knowledge, the limitations and implications of both methods have not been thoroughly examined.

3.1 Scaling back update in iterations

210 SU scales back the update (Eq. 7) with a scaling factor λ (Bethke, 2007; Hammond, 2003) such that

$$\mathbf{c}^{k+1,p+1} = \mathbf{c}^{k+1,p} - \lambda \delta \mathbf{c}^{k+1,p} > 0, \quad (13)$$

where

$$\lambda = \alpha \min \left[1, \frac{\mathbf{c}^{k+1,p}(i)}{\delta \mathbf{c}^{k+1,p}(i)} \right] \quad (14)$$

215 for positive $\delta \mathbf{c}^{k+1,p}(i)$ and $i = 1$ to m , with m as the number of species times the number of numerical grid cells. With SU, the concentration of the species that is going negative decreases by $(1 - \alpha)$ times in each iteration instead. This can be shown by solving the zero-order uptake problem $dc/dt = -1$: $c^{k+1} = c^k - \Delta t$ when $\Delta t \geq c^k$; otherwise, $\lambda = \alpha c^k / \Delta t$, and $c^{k+1} = (1 - \alpha)c^k$. With a default $\alpha = 0.99$ in PFLOTRAN, each iteration reduces the concentration by 100 times. With
220 multiple iterations, the concentration can approach machine precision or 0.

If $\mathbf{c}^{k+1,p}(i)$ is 0 (or below the machine precision), and $\delta \mathbf{c}^{k+1,p}(i) > 0$, then $\lambda = 0$, and the update is limited to 0. Even if $\lambda = 0$ occurs in only one grid cell for only one species, the update for all of the species and all of the grid cells are constrained to 0, and the residual will not be decreased to satisfy Eqs. (8 or 9) to achieve convergence. If the iteration is deemed converged because the scaled
225 update is 0, and Eq. (10) is met, the calculation will march through this time step without any change in the concentrations, numerically stopping all reactions. This can continue for many time steps until $\delta \mathbf{c}^{k+1,p}(i)$ becomes negative.

Application of a very small scaling factor λ due to decrease of a small concentration for one species may have a similar consequence: the iteration may not decrease the residual $f(\mathbf{c}^{k+1,p})$ or the
230 iteration may not converge because Eqs. (8 or 9) are not met. If the iteration is considered converged because of too small an update $\lambda \delta \mathbf{c}^{k+1,p}$ (Eq. 10 is satisfied), the scaling factor λ (e.g., 10^{-10}) may correctly limit the consumption reaction rates to account for availability limitation, but wrongly limit the production rate in the time step. This can be illustrated by adding to the zero-order uptake problem $dc/dt = -1$ an independent zero order production $de/dt = 1$: when $\Delta t \geq c^k$, $\lambda = \alpha c^k / \Delta t$,
235 $c^{k+1} = (1 - \alpha)c^k$, $e^{k+1} = e^k + \alpha c^k$ rather than $e^{k+1} = e^k + \Delta t$. If $c^k = 0$, SU numerically stops the independent production reaction.

To avoid excessive numerical error, PFLOTRAN reports an error and exits when $\lambda < \lambda_{\min}$, with a default $\lambda_{\min} = 10^{-10}$. This translates the accuracy issue into a stability issue. It is necessary to investigate SU to resolve both the accuracy and the stability issue.

240 3.2 Log transformation

LT is widely used in geochemical codes for describing highly variable concentrations for primary species such as H^+ or O_2 that can vary over many orders of magnitude as pH or redox state changes

without the need to use variable switching. It is also used to enforce positivity (Bethke, 2007; Hammond, 2003; Parkhurst and Appelo, 1999). Instead of solving Eq. (4) for \mathbf{c}^{k+1} using Eqs. (5,6,7), LT 245 solves for $(\ln \mathbf{c}^{k+1})$ from

$$\mathbf{J}_{\ln}(i,j) = \frac{\partial \mathbf{f}(i)}{\partial \ln(\mathbf{c}(j))} = \mathbf{c}(j) \frac{\partial \mathbf{f}(i)}{\partial \mathbf{c}(j)} = \mathbf{c}(j) \mathbf{J}(i,j), \quad (15)$$

$$\delta \ln \mathbf{c}^{k+1,p} = \mathbf{J}_{\ln}^{-1} \mathbf{f}(\mathbf{c}^{k+1,p}), \quad (16)$$

and

$$250 \quad \mathbf{c}^{k+1,p+1} = \mathbf{c}^{k+1,p} \exp[-\delta \ln(\mathbf{c}^{k+1,p})]. \quad (17)$$

One downside is apparent from Eq. (15): suppose $\mathbf{c}^{k+1,p}(j)$ is 10^{-10} ; $\mathbf{J}(i,j)$ (column j of the Jacobian) decreases by 10^{10} times to $\mathbf{J}_{\ln}(i,j)$. As a result, the condition number of the Jacobian matrix may increase by orders of magnitude, which may constrain the time step size to be substantially reduced, compared to the case without LT. Secondly, the small eigenvalues may result in large 255 $\delta \ln \mathbf{c}^{k+1,p}$, which may cause overshooting to an unrealistically large concentration (positive update), or essentially 0 concentration (negative update), or even overflow in the exponential function in Eq. (17). To prevent these problems, PFLOTRAN limits the update to

$$\delta \ln(\mathbf{c}^{k+1,p}) = \text{sign}[\delta \ln(\mathbf{c}^{k+1,p})] \min[\text{abs}(\delta \ln \mathbf{c}^{k+1,p}), \delta_{\ln,\max}] \quad (18)$$

with a default $\delta_{\ln,\max} = 5$. While SU limits the positive update to avoid negative concentration, 260 LT constrains both positive and negative update to prevent unrealistically low and high concentration. Thirdly, LT does not prevent 0 concentration per se: a number of iterations with positive $\delta \ln \mathbf{c}^{k+1,p}(j)$ update is likely to bring $\mathbf{c}^{k+1,p+1}(j)$ to be below machine precision or 0. With zero concentration, \mathbf{J}_{\ln} becomes singular, and the numerical solution fails. These can be shown by solving $dc/dt = -1$ in the log transformed form $d \ln c/dt = -1/c$: $c^{k+1} = c^k e^{-\Delta t/c^{k+1}}$. LT converts 265 the linear problem that does not require iteration to a nonlinear problem that needs to be solved iteratively. As c^{k+1} becomes small, Δt has to be decreased accordingly, or the concentration goes to below machine precision and $c^{k+1} = 0$ causes division by 0 overflow.

3.3 Downregulation of reaction rate

Even though ensuring nonnegativity, the concentrations can become very small or essentially 0 using 270 either SU or LT. With 0 or near 0 concentrations, the scaling factor for SU is small or 0, or the time step sizes for LT are too small if LT does not fail due to a singular Jacobian matrix. Both approaches require the solution to the mathematical representation itself be positive. To obtain such a mathematical representation, it is necessary to downregulate reaction rates to represent the limitation

of the availability of each reactant on the reaction rate. In the geochemical modeling literature, this
 275 is mostly represented by a rate limiting function as a function of concentration in each reaction
 for each reactant. CLM downregulates demand (consumption) as a function of rate (demand-based competition). We examine downregulation of consumption as a function of concentration (DC) and
 rate (DR) for use with SU or LT to address the nonphysical solution negativity.

3.3.1 Downregulation of consumption as a function of concentration

280 The first-order decay problem (Eqs. A1, A4, A7, A9) is nonnegative. This can be shown by solving
 the first-order problem $dc/dt = -c$ using the backward Euler method: $c^{k+1} = c^k/(1 + \Delta t)$; the con-
 centration decreases but remains nonnegative. However, it can go to 0 (or below machine precision).
 To avoid 0 concentration, a residual term is often used to limit the decay to a residual concentration
 (Tang et al., 2013a). For example, Eq. (A1) becomes

285
$$\frac{d[\text{CN}_u]}{dt} = -k_d f_T f_w ([\text{CN}_u] - [\text{CN}_u]_r). \quad (19)$$

When the concentration goes below $[\text{CN}_u]_r$ (overshoots) in an iteration, Eq. (19) implies a hypothet-
 ical reverse reaction to bring it back to $[\text{CN}_u]_r$. An alternative is to introduce a cutoff, e.g., Eq. (A1)
 becomes

$$\frac{d[\text{CN}_u]}{dt} = -k_d f_T f_w [\text{CN}_u] f([\text{CN}_u]), \quad (20)$$

290 with $f([\text{CN}_u]) = 1$ when $[\text{CN}_u] \geq [\text{CN}_u]_r$, and 0 otherwise. It is simple but does not prevent $[\text{CN}_u]$
 from getting below $[\text{CN}_u]_r$ or 0 in theory. In addition, it introduces a discontinuity. A polynomial
 function can be used to smooth the cutoff

$$f([\text{CN}_u]) = 1 - \left[1 - \left(\frac{[\text{CN}_u] - [\text{CN}_u]_r}{[\text{CN}_u]_1 - [\text{CN}_u]_r} \right)^2 \right]^2. \quad (21)$$

This function varies from 0 at $[\text{CN}_u]_r$ to 1 at $[\text{CN}_u]_1$, with zero derivatives at both points. While not
 295 implying a nonphysical reverse reaction as Eq. (19),

$$\frac{df([\text{CN}_u])}{d[\text{CN}_u]} = 4 \frac{[\text{CN}_u] - [\text{CN}_u]_r}{([\text{CN}_u]_1 - [\text{CN}_u]_r)^2} \left[1 - \left(\frac{[\text{CN}_u] - [\text{CN}_u]_r}{[\text{CN}_u]_1 - [\text{CN}_u]_r} \right)^2 \right]. \quad (22)$$

Depending on $[\text{CN}_u]_1 - [\text{CN}_u]_r$, this cutoff does introduce a large derivative change during the transi-
 tion: $df([\text{CN}_u])/d[\text{CN}_u]$ varies from 0 to 10^8 for $[\text{CN}_u]_r = 10^{-10}$ and $[\text{CN}_u]_1 = 10^{-8}$ (Fig. 14). The
 maximum increases at about the same order of magnitude as the decrease of $[\text{CN}_u]_r$ and $[\text{CN}_u]_1$.
 300 Even though smoothed, the cutoff is still a sharp change. The smaller the cutoff concentrations, the
 sharper the transitions. Marching through a steep transition in time usually involves small time steps.
 In contrast, the residual concentration introduced in Eq. (19) does not adjust the derivative, which
 appears less nonlinear. Obviously, enforcing positivity even for a linear problem (here the first-order

rate) introduces nonlinearity into the numerical problem. A smaller threshold may lead to higher
 305 nonlinearity. For example, even though a NO_3^- concentration of 10^{-10} M may not be detectable, and is not any different from 10^{-15} M, introducing the cutoff of Eq. (21) with a cutoff 10^{-15} produces five orders of magnitude more increase in the derivative than a cutoff of 10^{-10} . In the case when extremely low concentration matters (e.g., O_2), enforcing positivity with the implicit time stepping and Newton-Raphson method is numerically challenging.

310 For the litter decomposition reactions (R7, R8, R9) that immobilize nitrogen, the rate formulae (Eqs. A1, 19,) do not account for the limitation of the reaction rate by the availability of nitrogen. They are zero order with respect to nitrogen. Mechanistically, a nitrogen-limiting function needs to be added to those formulae to represent the limitation of decreasing nitrogen concentration on decomposition rate (downregulation), for example,

$$315 \quad \frac{d[\text{CN}_u]}{dt} = -k_d f_T f_w ([\text{CN}_u] - [\text{CN}_u]_r) f([N]). \quad (23)$$

A widely used downregulation function is the Monod substrate limitation function (Hammond, 2003; Tang et al., 2013a):

$$f([N]) = \frac{[N]}{[N] + k_m}, \quad (24)$$

with half saturation k_m . In the case of $[N] = k_m$, $f([N]) = 0.5$. For $[N] \gg k_m$, Eq. (24) is zero
 320 order with respect to $[N]$ or has little impact on the decomposition reactions that immobilize N. For $[N] \ll k_m$, Eq. (24) approximates first order with respect to $[N]$ (Figure 15d). Nevertheless, since

$$\frac{df([N])}{d[N]} = \frac{k_N}{([N] + k_m)^2}, \quad (25)$$

the derivative increases to about k_m^{-1} as the concentration decreases to below k_m (Fig. 15). This is similar to the smoothed cutoff in Eq. (21) (Fig. 14): even though smoothed, it is still a steep
 325 transition.

To represent the threshold concentration beyond which certain microorganisms can not use certain electron donors (Fennell and Gossett, 1998), a residual concentration was added to Eq. (24):

$$f([N]) = \frac{[N] - [N]_r}{[N] - [N]_r + k_m}. \quad (26)$$

Similar to Eq. (19), this implies a nonphysical backward reaction when $[N] < [N]_r$. If we use the cutoff
 330 instead of a residual concentration, a combination of Eqs. (24) and (21) produces more nonlinearity, as evidenced in Fig. (16), which is likely to result in small time step sizes to march through these highly nonlinear regions when the concentration gets there.

The plant nitrogen uptake reactions (R13, R14) are of zero order, and substrate limiting functions need to be added as well. For both plant uptake and immobilization, we also have to distribute the

335 demands between NH_4^+ and NO_3^- . If we simulate the NH_4^+ limitation on plant uptake or immobilization with

$$R_a = R_p \frac{[\text{NH}_4^+]}{[\text{NH}_4^+] + k_m}, \quad (27)$$

the NO_3^- plant uptake or immobilization can be represented by

$$R_n = (R_p - R_a) \frac{[\text{NO}_3^-]}{[\text{NO}_3^-] + k_m} = R_p \frac{k_m}{[\text{NH}_4^+] + k_m} \frac{[\text{NO}_3^-]}{[\text{NO}_3^-] + k_m}. \quad (28)$$

340 This essentially assumes an inhibition of NH_4^+ on NO_3^- uptake or immobilization, and k_m becomes an inhibition coefficient. This simulates the observation that plant NO_3^- uptake rate remained low until NH_4^+ concentrations dropped below a threshold (Eltrop and Marschner, 1996).

For comparison with CLM, we examine the uptake rate as a function of demands and available concentrations:

$$345 f_{pi} = \frac{R_a + R_n}{R_p} = \frac{[\text{NH}_4^+]}{[\text{NH}_4^+] + k_m} + \left(1 - \frac{[\text{NH}_4^+]}{[\text{NH}_4^+] + k_m}\right) \frac{[\text{NO}_3^-]}{[\text{NO}_3^-] + k_m}. \quad (29)$$

As an example, we consider uptake $R_p = 10^{-9} \text{ M s}^{-1}$ from a solution with various $[\text{NH}_4^+]$ and $[\text{NO}_3^-]$ for a 0.5 h time step. With CLM, $f_{pi} = 1$ when $[\text{NH}_4^+] + [\text{NO}_3^-] \geq R_p \Delta t$; otherwise, it decreases with decreasing $[\text{NH}_4^+] + [\text{NO}_3^-]$ (Fig. 2). The new representation (Eqs. 27, 28) is generally similar, with $f_{pi} = 1$ or 0 when $[\text{NH}_4^+]$ or $[\text{NO}_3^-] \gg$ or $\ll k_m$. For the intermediate concentrations, 350 f_{pi} in the new scheme is less than or equal to that in CLM because NH_4^+ “inhibits” NO_3^- uptake. The difference decreases with decreasing k_m , apparently disappearing at $k_m = 10^{-10}$ (Fig. 3).

Various level of preferences of NH_4^+ over NO_3^- uptake were observed for plants (Pfautsch et al., 2009; Warren and Adams, 2007; Nordin et al., 2001; Falkengren-Grerup, 1995; Gherardi et al., 2013). The microbial uptake of inorganic and organic nitrogen species is similar (Fouilland et al., 355 Kirchman, 1994; Kirchman and Wheeler, 1998; Middelburg and Nieuwenhuize, 2000; Veuger et al., 2004). CLM implies a strong preference for NH_4^+ over NO_3^- . For example, if NH_4^+ is abundant, NO_3^- will not be taken. The new scheme allows the level of preference to be adjusted by varying k_m .

The nitrification reaction (R11) associated with decomposition to produce N_2O with the rate (Eq. 360 A5) appears as zero order as well and needs to be further downregulated as

$$\frac{d[\text{NH}_4^+]}{dt} = -2 \frac{d[\text{N}_2\text{O}]}{dt} = -f_{nm} f_T f_w f_{pH} \max(R_{nm} \frac{[\text{NH}_4^+]}{[\text{NH}_4^+] + k_m}, 0). \quad (30)$$

DC involves adding residual concentration and half saturations, which has the potential to provide mechanistic treatment of the processes. It also introduces a number of parameters that need to be determined. These parameters may not be well defined and can vary among different microbe and plant 365 species under various conditions across the globe. An alternative is to downregulate consumption as a function of rate (DR) like CLM demand-based competition.

3.3.2 Downregulation of consumption as a function of rate

As described in Appendix A5, CLM splits the available nitrogen to meet the demands by microbes (immobilization) and plants in proportion to the potential rates (Thornton and Rosenbloom, 2005).

- 370 Suppose that the demand (consumption, sink, including immobilization, plant uptake, nitrification, etc.) rate is R_{dp} ; the supply (source, production, including deposition, mineralization, etc.) is rate R_s , and the concentration is $[N]$ at the beginning of the time step, the demand is downregulated to

$$R_d = \min \left[R_{dp}, R_s + \frac{[N]}{\Delta t} \right]. \quad (31)$$

- As CLM4.5 ignores the supply term R_s (Oleson et al., 2013), ? suggest to include it. For a reaction 375 that is limited by multiple substrates (e.g., nitrogen and phosphorus), they use the minimum of the downregulated rates. Like the demand based competition in CLM, this is simple to implement, and prevents negative concentration when the explicit forward difference method is used. It is different for the backward Euler method. Applying to $dc/dt = -1$, $c^{k+1} = c^k - \Delta t$ for $c^k \geq \Delta t$; for $c^k < \Delta t$, $c^{k+1} = c^k / 2$: the concentration decreases by half in a time step. This is similar to SU with $\alpha = 0.5$, 380 which is suggested by Bethke (2007). DR essentially downregulates the demands using the first-order rate when nitrogen is limiting. Eq. (31) is similar to Eq. (24), except that Eq. (24) switches from zero to the first-order rate smoothly, while Eq. (31) has a discontinuity.

Implementation of DR in a geochemical code like PFLOTRAN involves separating the supply and consumption rates for each species in each reaction, and checking and conducting downregulation when necessary after contributions from all of the reactions are accumulated. It involves not 385 only the rate terms for the residual but also the derivative terms for the Jacobian. The complexity explodes when more species needs to be downregulated (e.g., NH_4^+ , NO_3^- , and organic N) and there are transformation processes among these species. This is shown in Appendix A5, which describes the implementation of downregulation of NH_4^+ and NO_3^- with a nitrification reaction from NH_4^+ 390 to NO_3^- . Basically, it becomes challenging to separate, track, and downregulate consumption and production rates for an indefinite number of species, and calculation of the Jacobian becomes convoluted. Clearly, this work diff from ? in that we use implicit time stepping while they use explicit time stepping.

4 Test problems, results, and discussions

- 395 We can use SU or LT with either DC or DR, or a combination of both, to enforce nonnegativity. SU has the potential to introduce numerical error due to false convergence when STOL is satisfied and the scaling factor λ is too small. Stopping the simulation when λ is smaller than λ_{\min} changes the accuracy issue into a stability or robustness issue. For both SU and LT, allowing for tiny time step sizes and an excessive number of time step cuts may transfer a stability issue into an efficiency issue.

400 We examine the causes of negative concentration; the advantages and disadvantages of SU, LT, DC, and DR; and the accuracy, stability, and efficiency issue using both simple test problems and coupled CLM-PFLOTRAN site simulations. For simple test problems, we assess the conditions under which large updates occur. With coupled CLM-PFLOTRAN spin-up simulations for arctic, temperate, and tropical sites, we assess the conditions when the nonphysical solution negativity arises by relaxing 405 the downregulation on nitrogen consumption (decreasing half saturation). Spreadsheet, python scripts, and PFLOTRAN input files for these simple test problems and for producing figures are provided as supplemental information.

Our implementation of CLM biogeochemistry introduces mainly two parameters: half saturation k_m and residual concentration. A wide range of k_m values were reported for NH_4^+ , NO_3^- , and organic 410 nitrogen for microbes and plants. The median, mean, and standard deviations range from $10 \sim 100$, $50 \sim 500$, and $10 \sim 200 \mu\text{M}$, respectively (Kuzyakov and Xu, 2013). Reported residual (threshold) concentrations are limited and are considered to be 0 (e.g., HØGh-Jensen et al., 1997), likely because 415 of the detection limits of the analytical methods. The detection limits are usually at the μM level, while up to the nM level was reported (Nollet and De Gelder, 2013). In Ecosys, the k_m is 0.40 and 0.35 gN m^{-3} , and the residual concentration is 0.0125 and 0.03 gN m^{-3} (Grant, 2013) for NH_4^+ and NO_3^- for microbes. Depending on the moisture content, say 10, 100, and 1000 L m^{-3} for a dry, wet, and saturated case, these k_m values roughly translate to 10^{-3} , 10^{-4} , and 10^{-5} M . We start with $k_m = 10^{-6} \text{ M or mol m}^{-3}$, and residual concentration $10^{-15} \text{ M or mol m}^{-3}$ for plants and microbes. To further investigate the nonphysical solution negativity for the current study and 420 for future application for other nutrients (e.g., H_2 and O_2) where the concentrations can be much lower, we examine k_m from 10^{-3} to 10^{-12} in our test problems. The k_m is expected to be different for different plants, microbes, and for NH_4^+ and NO_3^- , and different values can be assigned in the input file in our implementation. we do not differentiate them in this work as we focus on numerical issues.

425 **4.1 Plant nitrogen uptake, nitrification, and denitrification**

It was observed that plants can decrease nitrogen concentration to below detection limits in hours (Kamer et al., 2001). Plant nitrogen uptake is one of the major sinks for nitrogen in TEMs and contributes to decreasing nitrogen concentration numerically to 0 or negative. In CLM, the total plant nitrogen demand is calculated based on photosynthesized carbon allocated for new growth 430 and the C:N stoichiometry for new growth allocation, and the plant nitrogen demand from the soil is equal to the total nitrogen demand minus retranslocated nitrogen stored in the plants (Oleson et al., 2013). The CLM calculated rate is provided as an input to PFLOTRAN, which is constant in a 0.5 h time step. Without downregulating plant nitrogen uptake rate, nitrogen concentration is likely to go negative when the net consumption rate overwhelms a low available concentration. 435 As the Monod substrate limiting function is the most widely used downregulation function, we

examine the numerical solutions, beginning with the numerical issues during the iteration processes. Incrementally, we add first order reactions (e.g., nitrification, denitrification, and plant NO_3^- uptake) to look into these issues in increasingly complex systems.

4.1.1 Plant NH_4^+ uptake (Test 1)

- 440 We consider the plant NH_4^+ uptake reaction (R13) with the rate R_a downregulated by the Monod substrate limiting function:

$$\frac{d[\text{NH}_4^+]}{dt} = -R_a \frac{[\text{NH}_4^+]}{[\text{NH}_4^+] + k_m} = -R_{at}. \quad (32)$$

As an analytical solution is not available, discretizing Eq. (32) using the backward Euler method, it becomes

$$445 [\text{NH}_4^+]^{k+1} + (k_m + R_a \Delta t - [\text{NH}_4^+]^k) [\text{NH}_4^+]^{k+1} - k_m [\text{NH}_4^+]^k = 0. \quad (33)$$

The two roots are

$$[\text{NH}_4^+]^{k+1} = 0.5 \left[[\text{NH}_4^+]^k - k_m - R_a \Delta t \pm \sqrt{([\text{NH}_4^+]^k - k_m - R_a \Delta t)^2 + 4k_m [\text{NH}_4^+]^k} \right]. \quad (34)$$

- One root is positive, and the other is negative (not physical). With the positive root, $[\text{NH}_4^+]^{k+1} \rightarrow 0$ when $[\text{NH}_4^+]^k \rightarrow 0$, or $R_a \Delta t \rightarrow \infty$. As $k_m \rightarrow 0$, $[\text{NH}_4^+]^{k+1} \rightarrow 0$ when $[\text{NH}_4^+]^k \leq R_a \Delta t$. If we 450 replace $[\text{NH}_4^+]$ with $[\text{NH}_4^+] - [\text{NH}_4^+]_r$ in Eqs. (32) and (34), $[\text{NH}_4^+]^{k+1} \rightarrow [\text{NH}_4^+]_r$ rather than 0. We do not include the residual concentration in the simple test problems for simplicity in this subsection. Ignoring the negative root, the representation of plant NH_4^+ uptake by Eq. (32) ensures $[\text{NH}_4^+]^{k+1} \geq [\text{NH}_4^+]_r$.

Solving Eq. (32) using the Newton-Raphson method from time step k to $k+1$, the update is

$$455 \delta[\text{NH}_4^+]^{k+1,p} = \frac{\frac{[\text{NH}_4^+]^{k+1,p} - [\text{NH}_4^+]_k}{\Delta t} + R_a \frac{[\text{NH}_4^+]^{k+1,p}}{[\text{NH}_4^+]^{k+1,p} + k_m}}{\frac{1}{\Delta t} + R_a \frac{k_m}{([\text{NH}_4^+]^{k+1,p} + k_m)^2}}. \quad (35)$$

For the first iteration, $[\text{NH}_4^+]^{k+1,0} = [\text{NH}_4^+]^k$,

$$\xi = \frac{\delta[\text{NH}_4^+]^{k+1,1}}{[\text{NH}_4^+]^{k+1,0}} = \frac{\frac{1}{[\text{NH}_4^+]^k + k_m}}{\frac{1}{R_a \Delta t} + \frac{k_m}{([\text{NH}_4^+]^k + k_m)^2}}. \quad (36)$$

The update is a function of uptake rate (R_a), time step size (Δt), concentration ($[\text{NH}_4^+]^k$), and half saturation (k_m). For $R_a \Delta t$ from 0 to ∞ , ξ increases from 0 to $1 + [\text{NH}_4^+]/k_m$. With $[\text{NH}_4^+]^k =$

460 10^{-6} M, and $k_m = 10^{-6}$ M, the update is less than $[\text{NH}_4^+]^k$ when $R_a\Delta t \leq 5 \times 10^{-6}$ M (say using CLM $\Delta t = 1800$ s, $R_a \leq 2.8 \times 10^{-9}$ mol s $^{-1}$, Fig. 4); when $R_a\Delta t$ increases, the update increases, with an upper limit of 2, suggesting that large time step size and uptake rate alone usually do not lead to an excessively large update or a small scaling factor. For $[\text{NH}_4^+]^k$ from 0 to ∞ , ξ starts from $R_a\Delta t/(k_m + R_a\Delta t)$, increases to peak at $\sqrt{R_a\Delta t/k_m}/2$ when $[\text{NH}_4^+] = \sqrt{k_m R_a \Delta t} - k_m$, and
 465 then decreases to 0. With $k_m = 10^{-6}$ M and $R_a\Delta t = 0.001$ M, ξ starts from ~ 1 , increases to peak at ~ 16 when $[\text{NH}_4^+]^k = 3 \times 10^{-5}$, and decreases to 0 as $[\text{NH}_4^+]^k \rightarrow \infty$. For k_m from ∞ to 0, ξ increases from 0 to $R_a\Delta t/k_m$. With $R_a\Delta t = 10^{-3}$, and $[\text{NH}_4^+]^k = 10^{-6}$, the update increases several orders of magnitude as k_m decreases from 10^{-6} to 10^{-9} , with a limit of $\xi = 10^3$ (Fig.4). While the semi-analytical solution (Eq. 34) indicates that the problem itself is nonnegative, these
 470 calculations suggests that overshoot can occur, and large time step, uptake rate, low concentration and half saturation can contribute to large update that can exceed the available concentration by orders of magnitude.

Now we look into the iteration processes: the solution starts with an overshoot to 1.995×10^{-6} and converges to the positive semi-analytical solution 3.1127×10^{-5} (Eq. 34) in eight iterations
 475 when $R_a\Delta t = 0.001$ (Table 1). dR/dC changes from ~ 1 to 10^5 in the first iteration, although the change in the Jacobian is reduced due to a small $R_a\Delta t$. With $R_a\Delta t = 0.002$, the update δ is greater than $[\text{NH}_4^+]_k$; without scaling back the update, the solution converges to the negative solution -1.002×10^{-3} (Table 2, negative root from Eq. 34). Scaling back the update with $\alpha = 0.9999$, the concentration decreases by $1 - \alpha = 10^{-4}$ times in the first iteration rather than to negative root
 480 (Table 3). The solution converges to the positive root in seven iterations.

If LT is used with $R_a\Delta t = 0.002$, the solution oscillates and results in a δ of -1041.5 in the fifth iteration, which essentially makes the solution 0 (Table 4). Limiting $\delta \leq \delta_{\text{ln,max}}$, the solution converges to the semi-analytical solution (Eq.34) in 7, 7, 6, 5, 6, and 8 iterations with $\delta_{\text{ln,max}} = 2, 3, 4, 5, 6$, and 7, respectively. For $\delta_{\text{ln,max}} \geq 8$, the iteration oscillates and converges slowly. If we split
 485 $R_a\Delta t = 0.002$ into two steps, the first step takes seven iterations to converge, while the second step takes nine iterations, with $\delta_{\text{ln,max}} = 5$. These simulations show that limiting the update to be less than $\delta_{\text{ln,max}}$ is helpful for LT to use large time step sizes for efficiency.

Finally, we consider a PFLOTRAN simulation: a $1 \text{ m} \times 1 \text{ m} \times 1 \text{ m}$ grid cell, with 0.25 water content, initial $4 \mu\text{M}$ NH_4^+ , and a plant NH_4^+ demand 10^{-7} mol s $^{-1}$ ($\sim 3 \text{ mg d}^{-1}$, reported values
 490 for evergreen and deciduous forest range from $0.3 \sim 10 \text{ g m}^{-2}$ year, Chapin et al., 2011). It takes 10,000 s (2.78 h) to consume NH_4^+ . We use a time step of 0.5 h for a simulation duration of 10 h. Without downregulating the uptake rate, SU decreases $[\text{NH}_4^+]$ to 0 and then keeps it 0 as $\lambda = 0$. With LT, we obtain an accurate solution until it fails when the concentration goes to 0, and the Jacobian becomes singular.

495 Using SU with DC with $[\text{NH}_4^+]_r$ of 10^{-20} M (Eq. 26) and a half saturation k_m of $10^{-6}, 10^{-9}$, or 10^{-12} , the calculated concentration $[\text{NH}_4^+]$ is kept to be greater than or equal to 10^{-20} (Figure.

5). With a k_m of 10^{-6} , the calculated $[\text{NH}_4^+]$ is above 10^{-20} , and the update does not exceed the concentration in any iteration during the 10 h simulation duration. With a k_m of 10^{-9} and 10^{-12} , the update exceeds the concentration from time 2.5 h to 3.0 h. In the case of $k_m = 10^{-12} \text{ M}$ for the next time step, the two iterations decrease the concentration by 10,000 times, and the solution is deemed converged as the default STOL = 10^{-8} is met. This continues for another time step with one iteration (Fig. 5). In these two time steps, the solution does not converge to the exact solution. If we set the residual concentration to 10^{-15} , the false convergence results in a concentration below 10^{-15} (8.71×10^{-16}) in the first of the two time steps. If we set STOL = 10^{-50} to avoid the convergence due to Eq. (10), PFLOTTRAN cuts the time step sizes and quits due to too many cuts.

Using LT can avoid the false convergences in this example, but it requires more iterations, with 56/95, 36/110, and 32/87 for SU/LT for k_m values of 10^{-6} , 10^{-9} , and 10^{-12} M , respectively. These results demonstrate that SU ensures nonnegativity and allows large time step for efficiency at the risk of inaccuracy. LT is accurate but requires more iterations.

510 4.1.2 Plant NH_4^+ uptake and nitrification (Test 2)

Adding a nitrification reaction (R10) with a first-order rate, Eq. (32) becomes

$$\frac{d[\text{NH}_4^+]}{dt} = -R_a \frac{[\text{NH}_4^+]}{[\text{NH}_4^+] + k_m} - k_{nitr} [\text{NH}_4^+] = -R_{at} - R_{nitr}. \quad (37)$$

Discretizing the equation in time using the backward Euler method,

$$(1 + k_{nitr}\Delta t)[\text{NH}_4^+]^{k+1} + (k_m + R_a\Delta T + k_{nitr}k_m\Delta t - [\text{NH}_4^+]^k)\text{NH}_4^+^{k+1} - k_m[\text{NH}_4^+]^k = 0. \quad (38)$$

515 Denote $b = [\text{NH}_4^+]^k - (k_m + R_a\Delta T + k_{nitr}k_m\Delta t)$, the roots are

$$[\text{NH}_4^+]^{k+1} = \frac{b \pm \sqrt{b^2 + 4(1 + k_{nitr}\Delta t)[\text{NH}_4^+]^k k_m}}{2(1 + k_{nitr}\Delta t)}. \quad (39)$$

Similar to Eq. (32), one root is nonnegative. To solve the problem with the Newton-Raphson method, the equation is

$$\begin{bmatrix} \frac{1}{\Delta t} + J_{at} + J_{nitr} & 0 & 0 \\ -J_{at} & \frac{1}{\Delta t} & 0 \\ -J_{nitr} & 0 & \frac{1}{\Delta t} \end{bmatrix} \begin{pmatrix} \delta[\text{NH}_4^+]^{k+1,1} \\ \delta[\text{PlantA}]^{k+1,1} \\ \delta[\text{NO}_3^-]^{k+1,1} \end{pmatrix} = \begin{pmatrix} R_{at} + R_{nitr} \\ -R_{at} \\ -R_{nitr} \end{pmatrix}, \quad (40)$$

520 with $J_{at} = \frac{dR_{at}}{d[\text{NH}_4^+]} = R_a \frac{k_m}{([\text{NH}_4^+] + k_m)^2}$, and $J_{nitr} = \frac{dR_{nitr}}{d[\text{NH}_4^+]} = k_{nitr}$. The solutions are

$$\delta[\text{NH}_4^+]^{k+1,1} = \frac{R_{at} + R_{nitr}}{\frac{1}{\Delta t} + J_{at} + J_{nitr}}, \quad (41)$$

$$\delta[\text{PlantA}]^{k+1,1} = J_{at}\delta[\text{NH}_4^+]^{k+1,1} - R_{at} = -\frac{\frac{1}{\Delta t} + J_{nitr}}{\frac{1}{\Delta t} + J_{at} + J_{nitr}}R_{at} + \frac{J_{at}}{\frac{1}{\Delta t} + J_{at} + J_{nitr}}R_{nitr}, \quad (42)$$

and

$$\delta[\text{NO}_3^-]^{k+1,1} = J_{nitr}\delta[\text{NH}_4^+]^{k+1,1} - R_{nitr} = \frac{J_{nitr}}{\frac{1}{\Delta t} + J_{at} + J_{nitr}}R_{at} - \frac{\frac{1}{\Delta t} + J_{at}}{\frac{1}{\Delta t} + J_{at} + J_{nitr}}R_{nitr}. \quad (43)$$

525 It is not a surprise for $\delta[\text{NH}_4^+]^{k+1,1}$ to be positive as plant NH_4^+ uptake and nitrification consume NH_4^+ . It is a little surprising that a positive component, $\frac{J_{at}}{\frac{1}{\Delta t} + J_{at} + J_{nitr}}R_{nitr}$, is introduced to $\delta[\text{PlantA}]^{k+1,1}$ even though there is no reaction that consumes PlantA. Depending on the relative magnitude of the rates (R_{at} and R_{nitr}) and the derivatives (J_{at} and J_{nitr}), as well as time step size Δt and $[\text{NH}_4^+]^k$, the update can be positive, which can result in too small a scaling factor that causes
530 a nonphysical solution negativity if [PlantA] is very small. This demonstrates that products as well as reactants can be driven negative during the Newton-Raphson iterations (overshoot).

This can also be shown with another simple first-order reaction $A \rightarrow B$ with rate $k[A]$: taking out the equation for B, $-k\delta[A] + \delta[B]/\Delta t = -k[A]$, $\delta[B] = k\Delta t(\delta[A] - [A])$. Suppose $\delta[A] = 2 \times 10^{-6}$, $[A] = 10^{-6}$, and $k\Delta t = 10^{-3}$, then $\delta[B] = 10^{-9}$. If [B] is very small, say 10^{-20} , this results in a
535 $\lambda = 0.99 \times 10^{-11}$. This has an implication for DR: downregulating only some reactants may not be sufficient to guarantee positivity, while downregulating both reactants and products is complicated.

The update δNO_3^- can be positive, and cause negative consequence for the calculation as well. It can become worse when the same Monod substrate limiting function is used to further downregulate the nitrification rate like CLM demand based competition, namely, $R_{nitr} = k_{nitr}[\text{NH}_4^+] \frac{[\text{NH}_4^+]}{[\text{NH}_4^+] + k_m}$,
540 $J_{nitr} = k_{nitr} \frac{[\text{NH}_4^+]}{[\text{NH}_4^+] + k_m} + k_{nitr}[\text{NH}_4^+] \frac{k_m}{[(\text{NH}_4^+) + k_m]^2} = k_{nitr} \frac{[\text{NH}_4^+]}{[\text{NH}_4^+] + k_m} \left(1 + \frac{k_m}{[\text{NH}_4^+] + k_m}\right)$. For $[\text{NH}_4^+] \ll k_m$, this increases J_{nitr} approximately by the order of k_m^{-1} , which can result in an increase of the update.

4.1.3 Plant uptake, nitrification, and denitrification (Test 3)

Adding plant NO_3^- uptake reaction (R14) with rate $R_{nt} = R_p \frac{[\text{NH}_4^+]}{[\text{NH}_4^+] + k_m} \frac{[\text{NO}_3^-]}{[\text{NO}_3^-] + k_m}$, $J_{nt,n} = \frac{dR_{nt}}{d[\text{NO}_3^-]} =$
545 $R_p \frac{[\text{NH}_4^+]}{[\text{NH}_4^+] + k_m} \frac{k_m}{([\text{NO}_3^-] + k_m)^2}$, and $J_{nt,a} = \frac{dR_{nt}}{d[\text{NH}_4^+]} = \frac{dR_n}{d[\text{NH}_4^+]} \frac{k_m}{([\text{NH}_4^+] + k_m)^2} \frac{[\text{NO}_3^-]}{[\text{NO}_3^-] + k_m}$, and denitrification reaction (R12) with rate $R_{deni} = k_{deni}[\text{NO}_3^-]$, and $J_{deni} = \frac{dR_{deni}}{d[\text{NO}_3^-]} = k_{deni}$, the equation becomes

$$\begin{bmatrix} \frac{1}{\Delta t} + J_{at} + J_{nitr} & 0 & 0 & 0 \\ -J_{at} & \frac{1}{\Delta t} & 0 & 0 \\ -J_{nitr} + J_{nt,a} & 0 & \frac{1}{\Delta t} + J_{nt} + J_{deni} & 0 \\ -J_{nt,a} & 0 & -J_{nt,n} & 1/\Delta t \\ 0 & 0 & -0.5J_{deni} & 0 \end{bmatrix} \begin{pmatrix} \delta[\text{NH}_4^+]^{k+1,1} \\ \delta[\text{PlantA}]^{k+1,1} \\ \delta[\text{NO}_3^-]^{k+1,1} \\ \delta[\text{PlantN}]^{k+1,1} \\ \delta[\text{N}_2]^{k+1,1} \end{pmatrix} = \begin{pmatrix} R_{at} + R_{nitr} \\ -R_{at} \\ -R_{nitr} + R_{nt} + R_{deni} \\ -R_{nt} \\ -0.5R_{deni} \end{pmatrix}. \quad (44)$$

As a result,

$$\delta[\text{NO}_3^-]^{k+1,1} \left(\frac{1}{\Delta t} + J_{nt} + J_{deni} \right) = (J_{nitr} - J_{nt,a}) (R_{at} + R_{nitr}) \delta[\text{NH}_4^+]^{k+1,1} - R_{nitr} + R_{nt} + R_{deni}, \quad (45)$$

550 and

$$\delta[\text{PlantN}]^{k+1,1} / \Delta t = J_{nt,a} \delta[\text{NH}_4^+]^{k+1,1} + J_{nt,n} \delta[\text{NO}_3^-]^{k+1,1} - R_{nt}. \quad (46)$$

In addition to plant NH_4^+ uptake and nitrification, $\delta[\text{NO}_3^-]^{k+1,1}$ becomes a function of plant NO_3^- uptake and denitrification, and all of the rate coefficients and derivatives may contribute to a positive update that can result in too small a scaling factor. Even though the problem itself is nonnegative,
555 coupling these reactions together in the Newton-Raphson iteration does introduce the potential to produce relatively significant positive update for NO_3^- and PlantN. It worsens when the preference-based uptake of NH_4^+ over NO_3^- (Eqs. 27 and 28) brings in the impact of any rates related to NH_4^+ (including deposition, uptake, immobilization, etc.), with potentially large derivative terms for the off-diagonal entries in the Jacobian matrix. It is the nonlinearity introduced in the downregulation
560 and propagated through the reactions that causes the challenge. A smaller half saturation introduces a greater derivative change; therefore, it is more likely to cause the problem. These results also suggest that the likelihood for NO_3^- to go negative is greater than NH_4^+ , and PlantN is greater than PlantA as the latter are influenced by more rates and derivatives.

4.2 N immobilization, mineralization, and nitrification during decomposition (Test 4)

565 We further examine the implications of a small half saturation on the numerical solutions with a decomposition test problem. We consider a case of decomposing 0.2 M Lit1C + 0.005 M Lit1N to produce SOM1 with an initial 4 μM NH_4^+ using the reactions (R7 and R2) in the CLM-CN reaction network (Fig. 1) at first. Then we add the nitrification reaction (R11) with rate (Eq. 30) to examine the implications of a complex rate formula. We use PFLOTRAN with a fully saturated grid cell of 1
570 m and porosity of 0.25.

Lit1 decomposes fast at the beginning and then slows down as NH_4^+ is depleted (Fig. 6). The Lit1 decomposition rate is controlled by the mineralization rate from SOM1 decomposition. As the immobilization rate decreases with decreasing Lit1, $[\text{NH}_4^+]$ rebounds. For k_m of 10^{-6} , 10^{-9} , and 10^{-12} M, Lit1 and SOM1 dynamics are similar, but the $[\text{NH}_4^+]$ values are decreased to $\sim 10^{-8}$,
575 10^{-11} , and 10^{-14} M, respectively. The number of iterations for SU/LT is 76/169, 68/194, and 54/207 for the three k_m values. Obviously, smaller k_m results in lower $[\text{NH}_4^+]$ and more iterations.

The implication of $k_m = 10^{-12}$ becomes obvious when the nitrification reaction (R11) with rate (Eq. 30) is included. In the time step when the mineralization rate surpasses the immobilization, $\delta[\text{N}_2\text{O}] > [\text{N}_2\text{O}]$, and N_2O is lowered to 10^{-23} M in three iterations as STOL is met. In the next

580 time step, $\delta[N_2O] = \sim 10^{-13}$, resulting in a scaling factor λ of 10^{-10} that stops the simulation. Checking the calculations in the last iteration, the lower NH_4^+ concentration (2×10^{-13} M) introduces a derivative (6.94×10^{11}) into the column of the Jacobian with respect to NH_4^+ . Because N_2O production is a function of both immobilization and mineralization, a Monod substrate limiting function is added to downregulate the mineralization component (Eq. 30). In the row corresponding to
585 N_2O , the off-diagonal terms are nonzero in the entries with respect to NH_4^+ , Lit1C, Lit1N, and SOM1. Even though these values are relatively small because the fraction of net mineralization rate to N_2O is small (0.02), inversion of the Jacobian matrix results in substantial values in the row, and the 10^{-13} M update comes mainly from the entries with respect to Lit1C and Lit1N. This further illustrates that extremely small half saturation together with complex rate limiting formula can result
590 in large derivatives at small concentration, which may lead to overshoot that results in a small update scaling factor.

4.3 CLM-PFLOTRAN simulations

We examine the nonphysical solution negativity in the coupled CLM-PFLOTRAN simulations for arctic (US-Brw), temperate (US-WBW), and tropical (BR-Cax) AmeriFlux sites. The CLM-PFLOTRAN
595 simulations are run in the mode that PFLOTRAN only handles subsurface chemistry (decomposition, nitrification, denitrification, N plant uptake). For comparison, 1) depth and O_2 availability impact on decomposition, 2) cryoturbation, 3) SOM transport, and 3) nitrogen leaching are ignored by setting 1) decomp_depth_efolding to 10^6 m, o_scalar to 1, 2) cryoturb_diffusion, 3) som_diffusion, and 4)
600 sf_no3 and sf_sminn to 0. For CLM-PFLOTRAN simulations, $k_m = 10^{-6}$ and residual concentration 10^{-15} are used for the base case. The nonphysical solution negativity is assessed in particular by relaxing the downregulation (decreasing k_m). Nitrogen is the focus as it is the rate limiting nutrient in CLM4.5 biogeochemistry. Spin-up simulations are used because they are generally more likely to face a nonphysical solution negativity because the simulations start far away from equilibrium. In these site simulations, PFLOTRAN uses the same 10 layer grid for the 3.8 m one-dimensional
605 column as CLM. The simulation duration is 500, 300, and 300 year for the arctic, temperate, and tropical sites as the system roughly reaches steady state within these simulation durations.

4.3.1 Site descriptions

The US-Brw site (71.35N,156.62W) is located near Barrow, Alaska. The mean annual temperature, precipitation, and snowfall are $-12^\circ C$, 11 cm, and 69 cm, respectively (1971 ~ 2000) (Lara et al.,
610 2012). The landscape is poorly drained polygonized tundra. The maximum thaw depth ranges from 30 to 40 cm, and the snow free-period is variable in length but generally begins in early June and lasts until early September (Hinkel and Nelson, 2003). The area is composed of several different representative wet-moist coastal sedge tundra types, including wet sedges, grasses, moss, and assorted lichens. The leaf area index (LAI) is ~ 1.1 .

615 The US-WBW site (35.96N, 84.29W) is located in the Walker Branch Watershed in Oak Ridge,
Tennessee (Hanson and Wullschleger, 2003). The climate is typical of the humid southern Ap-
palachian region. The mean annual precipitation is \sim 139 cm, and the mean median temperature
is 14.5 °C. The soil is primarily Ultisols that developed in humid climates in the temperate zone
on old or highly weathered material under forest. The temperate deciduous broadleaf forest was
620 regenerated from agriculture land 50 years ago. LAI is \sim 6.2 (Hanson et al., 2004).

The BR-Cax site (-1.72N, -51.46W) is located in the eastern Amazon tropical rainforest. The
mean annual rainfall is between 2000 and 2500 mm, with a pronounced dry season between June
and November. The soil is a yellow oxisol (Brazilian classification latossolo amarelo) with a thick
stony laterite layer at 3 \sim 4 m depth (da Costa et al., 2010). The vegetation is evergreen broadleaf
625 forest. The LAI is 4 \sim 6 (Powell et al., 2013).

4.3.2 Base case simulation results

For CLM-PFLOTRAN base case simulations, we use DC and LT because DC is the general geo-
chemical modeling approach and is rigorous, and LT is less likely to cause numerical error than
SU. The site climate data from 1998 to 2006, 2002 to 2010, and 2001 to 2006 are used to drive
630 the spin-up simulation for the arctic, temperate, and tropical sites, respectively. This introduces a
multi-year cycle in addition to the annual cycle (Figs. 7, 8, 9). Overall, CLM-PFLOTRAN is close
to CLM4.5 in predicting LAI and nitrogen distribution among vegetation, litter, SOM, NH_4^+ and
 NO_3^- pools for the arctic (Fig. 7), temperate (Fig. 8), and tropical site (Fig. 9). CLM4.5 does reach
equilibrium earlier than CLM-PFLOTRAN as the latter represents slightly more inhibition on plant
635 nitrogen uptake, depending on the half saturation. The impact is most obvious for LitN, NH_4^+ , and
 NO_3^- in the tropical site (Fig. 9). Because the nitrogen demand competition scheme implemented in
CLM-PFLOTRAN is different from that in CLM4.5, we do not expect identical results as Fang et al.
(2013).

The arctic site shows a distinct summer growing season (Fig. 7): LAI and VEGN jump up at the
640 beginning, then level off, and drop down at the end of the growing season when LITN jumps up due
to litter fall. NH_4^+ and NO_3^- drop to very low level at the beginning of growing season and accumu-
late at the other times. In addition to a longer growing season than the arctic site, the temperate site
shows more litter fall by the end of the growing season as it is a temperate deciduous forest, which
introduces immobilization demand that further lowers NH_4^+ and NO_3^- concentrations (Fig. 8e inset).
645 The seasonality is much less apparent in the tropical site than in the arctic and temperate sites. LAI,
VEGN, LITN, and SOMN accumulate with less seasonal variations to reach an equilibrium. It takes
much longer simulation duration to spin up the simulation for the arctic site than the temperate and
tropical sites because the arctic site receives less solar radiation.

Except for the tropical site where the higher k_m of 10^{-3} mol m $^{-3}$ results in lower immobilization,
650 higher accumulation of LITN, and higher $[\text{NH}_4^+]$ and $[\text{NO}_3^-]$ during the spinup (Fig. 9), the range of

k_m values (10^{-3} , 10^{-6} , and $10^{-9} \text{ mol m}^{-3}$) generally has limited impact on the overall calculations except that the nitrogen concentrations drop lower with lower k_m values (e.g., inset in Figs. 7e,f, 8e), which is similar to Fig. (6). The lack of sensitivity is because these very low concentrations do not make up a mass of nitrogen that is significant enough to influence the carbon and nitrogen cycle. However, as a small k_m value means weak downregulation and steep transition between zero order and first order, it has implications on the accuracy, stability, and efficiency of the numerical solutions.

4.3.3 Efficiency

We use OIC (ORNL Institutional Cluster phase5 esd13q) for the comparison of computing time for the three sites using DC or DR with SU or LT. The results suggest that SU takes about 30~80% more time than CLM, and LT costs about two to four times that of CLM (Table 5). For LT with DC, the computing time increases with decreasing k_m . This is expected because a smaller k_m may require smaller time step size to march through steeper transition. The computing time appears not to be infeasible. The comparison between DC and DR is mixed. This is because DC has more complicated substrate limiting representation that requires smaller time step sizes to march through steep transitions, while DR has simpler substrate limiting representation, but a discontinuity that may require more iterations. We expect that CLM-PFLOTRAN will require more computational cost as more complex biogeochemical processes are represented, transport is added, and thermal hydrology (including freeze and thaw) are incorporated. Future code optimization for performance on next-generation supercomputers is expected to mitigate the computational cost.

4.3.4 Accuracy

We use the tropical site to demonstrate the accuracy issue by SU (scaling update); i.e., the small scaling factor (λ) may not only limit N consumption (immobilization and uptake) to account for availability limitation but also “inhibit” accumulation from mineralization, deposition, and fixation. The latter is unintended consequence and can introduce numerical error when the solution is considered converged because STOL is met. With $k_m = 10^{-3} \text{ mol m}^{-3}$, the LAI, VEGN, LITN, SOMN, NH_4^+ , and NO_3^- are similar to that calculated using LT (Fig. 9 vs. 10). With decreasing k_m , the results diverge by SU but not by LT. With k_m of $10^{-6} \text{ mol m}^{-3}$, much less nitrogen is predicted to accumulate with SU than with LT. Checking NH_4^+ and NO_3^- concentration in the first year, SU calculation is similar to LT when NH_4^+ and NO_3^- are abundant due to nitrogen mineralization from SOM4 decomposition at early times (Fig. 11). As nitrogen becomes limiting at late times due to increased plant nitrogen demand, NH_4^+ and NO_3^- accumulate lower by SU than by LT. Further checking into the daily cycles (Fig. 11 inset) reveals that NH_4^+ and NO_3^- accumulate during the night when photosynthesis and plant nitrogen uptake pause. As the sun rises, photosynthesis and plant nitrogen uptake resume, decreasing

nitrogen concentrations to very low level, limiting further uptake. As a result, nitrogen rebounds and then decreases again until sunset. From day 226 to 230, SU calculations are only slightly lower than LT calculations during the rebound. From day 250 to 254, the SU calculated rebounds are much lower than LT calculations. From day 295 to 300, accumulation during both night and day
690 are decreased. Overall, NH_4^+ and NO_3^- accumulation appear to be numerically “inhibited” when the system becomes increasingly nitrogen limiting and when SU is used. As a result, the mass balance error shots up during the nitrogen limiting periods (Fig. 12).

Finally checking nitrogen dynamics between day 250 and 254, these “inhibited” intervals in Fig. (11) coincide with the concentration valleys in the diagnostic species N_2Od , which is used to track
695 N_2O production (reaction R11) due to decomposition (Eq. 30, Fig. 13). At the beginning of each CLM 0.5 h time step, we reset $[\text{N}_2\text{Od}]$ to 10^{-10} in PFLOTRAN so that it can be used to calculate the reaction rate for CLM (instead of saving concentration in previous time step) As we do not have any consumption reaction for N_2Od , the decreases are purely numerical. The contribution of the derivatives of the rate (Eq. 30) results in a large enough positive update to N_2Od , which results in
700 a small scaling factor, and the solution is considered converged due to less than STOL update. This small scaling factor and false convergence result in the “inhibition” of NH_4^+ and NO_3^- production, and manifest as much less nitrogen accumulation in Fig. (10). If we remove the contribution of the derivatives for Eq. (30) for the entries with respect to N_2Od from the Jacobian, the “inhibition” disappears and SU results become close to LT (Fig. 13). If we decrease STOL from 10^{-8} to 10^{-50} , and
705 λ_{\min} from 10^{-10} to 10^{-50} , the false convergence occurs less often and the difference from LT decreases. However, the mass balance error remains (Fig. 12). This can also be mitigated by increasing the value from 10^{-10} to 10^{-6} that we reset these diagnostic species concentrations. Resetting the concentrations of these diagnostic species to low values in each time step does magnify the issue.
When these optional species are optioned out by excluding them from the species list in the input
710 file, the chance for the issue to occur is very much decreased. Nevertheless, as long as low concentrations are produced, which is expected as competition for substrates or nutrients there is common, there is a possibility for the issue to emerge even with realistic half saturation values.

An alternative to mitigate the issue is to use DR rather than DC. The rate formulae for DR can be very simple (no need for substrate limiting function). Because we use k_m to distribute nitrogen
715 demand between NH_4^+ and NO_3^- (Eqs. 27 and 28) for plant nitrogen uptake and immobilization, our implementation ends up with the difference between DC and DR as that DR does not have NO_3^- substrate limiting terms and uses Eq. (31) for downregulation of both NH_4^+ and NO_3^- . With DR, the numerical error is much reduced (not shown). However, it increases slightly with decreasing k_m when comparing with LT (not shown). These results show that decreasing the complexity of the rate
720 limiting representation helps reducing the nonphysical solution negativity for SU.

SU limits the update to prevent negative concentration (Eq. 13), and LT

4.3.5 Stability and robustness

PFLOTRAN may stop CLM-PFLOTRAN run due to 1) too small a scaling factor for SU to avoid excessive numerical error, 2) too small a time step size or too many time step cuts for either SU or

725 LT, and 3) singular Jacobian matrix for LT.

With SU and DC, the simulations run to conclusion for $k_m = 10^{-3}$, 10^{-6} , and $10^{-9} \text{ mol m}^{-3}$ but abort for $k_m = 10^{-12}$ for all of the three sites (Table 6). The reasons for the unfinished runs are too small a scaling factor for NO_3^- (Table 6). As indicated in Test 3, it is not surprising to see positive updates to NO_3^- as they depend on source and sink terms not only for NO_3^- but also for NH_4^+

730 because of the nitrogen demand distribution scheme (Eq. 28) for plant uptake and immobilization.

With smaller k_m , the derivative of the substrate limiting function (Eq. 25) becomes bigger when the concentration is lower, and the off-diagonal entries in the Jacobian matrix become more dominant, increasing the probability of producing positive update. When a greater than $[\text{NO}_3^-]$ update is produced,

735 $[\text{NO}_3^-]$ is expected to decrease by $1-\alpha$ times (0.01 by default) for each subsequent iterations, making it lower than the residual concentration (10^{-15}). If the λ is not greater than 10^{-10} , and the solution may be considered converged because STOL is satisfied, $[\text{NO}_3^-]$ can be very low, much below residual concentration (10^{-26}) in Table 6. With such low concentrations, a positive update

740 can make the scaling factor to be less than 10^{-10} . The arctic site simulation aborts at a much later time than the temperate and tropical site because the uptake and immobilization rate is much smaller in the former site.

A lower STOL can be used to avoid or mitigate the false convergence. With $\text{STOL} = 10^{-12}$, the simulations abort for $k_m = 10^{-3}$, 10^{-6} , and $10^{-9} \text{ mol m}^{-3}$ for the three sites due to too big an update for the diagnostic variables (PlantN, DeniN, or N₂Od, Table 6). For each time step, these concentrations start with 10^{-10} ; with an update as big as 10^{-6} , the concentration can be lowered in

745 several iterations using Eq. (13) to be below 10^{-10} times the update, resulting too small a scaling factor.

Removing the contribution of the derivatives to entries for these diagnostic species in the Jacobian can mitigate this stability and accuracy issue but may slow down the convergence or cause numerical errors. Increasing the reset value from 10^{-10} can mitigate the issue. However, as long as there is a very low concentration for any species, there is a possibility for this issue to occur.

750 Instead of aborting the run when the scaling factor is less than the minimum allowable value λ_{min} , an alternative is to consider the iteration diverges and return to the time stepping subroutine to cut time step size to increase accuracy. This mitigates the stability and accuracy challenge at the expense of computing time. Our results show the default $\lambda_{min} = 10^{-10}$ can result in excessive error even when STOL is extremely small. It is not clear how large a λ_{min} value can insure accuracy without introducing unnecessary computing time. For this reason, we caution against use of SU.

Similar to SU, the simulations using LT run to conclusion for $k_m = 10^{-3}$, 10^{-6} , and $10^{-9} \text{ mol m}^{-3}$ but abort for $k_m = 10^{-12}$ for all of the three sites. The runs abort at 21.6, 2.46, and 1.1 year for the arctic, temperate, and tropical site because the number of time step cuts for one time step exceeds

MAX_CUT = 16 (default). Increasing MAX_CUT to 50, the simulations run to conclusion with
760 longer computing time (Table 5). Looking into the reason for time step cuts, it usually involves iteration with NO_3^- concentration oscillation between the first order and zero order (Fig. 15b, for example, between 1.69×10^{-11} and 1.14×10^{-13} in the sixth layer in 0.5 year for BR-Cax site). While requiring an excessively large MAX_CUT, all of the simulations conclude with less than a 20% increase of computing time for k_m of 10^{-12} over 10^{-9} . These results suggest that log transformation together with downregulation with reasonable half saturation and residual concentration
765 can provide accurate, stable, and feasibly efficient solutions for CLM-PFLOTRAN biogeochemistry simulations.

5 Summary and Conclusions

We implement CLM biogeochemistry, specifically, CLM-CN decomposition, nitrification, denitrification,
770 and plant nitrogen uptake reactions in CLM-PFLOTRAN. As CLM uses explicit time stepping (forward difference) and demand-based competition, the concentration is always nonnegative. PFLOTRAN uses implicit time stepping (backward Euler method) and Newton-Raphson method; the concentration can become negative, which is not physical, may cause numerical instability, and introduce numerical error.

775 Both scaling back update in each iteration and log transformation can enforce nonnegativity. SU allows large time step sizes to achieve efficiency, but may introduce excessive numerical error if the scaling factor is small and the iterations are considered converged due to small updates. Log transformation involves multiplication of the Jacobian matrix by the concentration vector, decreasing the condition number by orders of magnitude as the concentration can be low. As a result, LT often
780 decreases the time step size and increases computational cost. Neither SU nor LT prevents too small or 0 concentrations. When the concentration becomes too small and essentially 0, SU may stop all reactions by a small positivity update caused by consumption, numerical overshoot, or truncation error and LT can fail due to too stiff or singular Jacobian matrix. Both SU and LT require that the limitation of reactant availability on reaction rates to be represented such that solution to the
785 mathematical representation does not introduce negative or 0 concentrations.

The first-order rate accounts for limitation of the reactant availability on the reaction rate, and the solution is nonnegative. Adding a residual concentration makes it positive. For the zero-order rate (or when the rate is not a function of a reactant), the Monod substrate limiting function provides a smooth transition from a zero order when the reactant is abundant to a first order when the
790 reactant becomes limiting. The downregulation relaxes with decreasing half saturation and residual concentration and disappears when both are 0.

Our CLM-PFLOTRAN spin-up simulation at an arctic, temperate, and tropical site indicates that accurate and stable solution can be achieved with log transformation with two to three times the

computing time of CLM4.5 for a range of half saturation values from 10^{-3} to 10^{-9} and a residual
795 concentration of 10^{-15} for nitrogen. With half saturation of 10^{-12} , the number of maximum time
cuts has to be increased from the default 16 to accommodate for small time step sizes to resolve
small concentration changes in the transition of zero and first-order rate. The computing time in-
crease from the half saturation of 10^{-12} to 10^{-9} is less than 20%. As physical half saturation ranges
800 from 10^{-5} to 10^{-6} M for nitrogen, and the detection limits are often above 10^{-9} M, log trans-
formation together with downregulation by reasonable half saturation and residual concentration is
expected to provide an accurate, stable, and efficient solution for CLM-PFLOTRAN implementation
for current CLM biogeochemistry. As more substrate limiting processes, such as labile C, P, O₂, and
H₂, are implemented with lower half saturation and residual concentration, and more complicated
rate relationship, the maximum allowable time step cut may need to be increased, and the computing
805 time is expected to increase.

6 Code availability

PFLOTRAN is an open-source software. It is distributed under the terms of the GNU Lesser General
Public License as published by the Free Software Foundation either version 2.1 of the License, or
any later version. It is available at <https://bitbucket.org/pfotran>.

810 7 Author contribution

G. B., B. A., R. M., J. K., and F. H. developed the CLM-PFLOTRAN framework that this work
built upon. F.Y., G.T., G. B., and X.X. added biogeochemistry to the CLM-PFLOTRAN interface. F.
Y. proposed the nitrification and denitrification reactions and rate formulae. G. T., F. Y., and X. X.
implemented the CLM biogeochemistry in PFLOTRAN under guidance of G. H., P. L., S. P., and
815 P.T. G.T. prepared the manuscript with contributions from all co-authors. G. T., F. Y., G. B., and G.H.
contributed equally to the work.

Acknowledgements. Thanks to Nathaniel O. Collier at ORNL for many discussion that contributed significantly
to this work. Thanks to Kathie Tallant and Cathy Jones at ORNL for editing service. This research was funded by
the U.S. Department of Energy, Office of Sciences, Biological and Environmental Research, Terrestrial Ecosys-
820 tem Sciences and Subsurface Biogeochemical Research Program, and is a product of the Next-Generation
Ecosystem Experiments in the Arctic (NGEE-Arctic) project. ORNL is managed by UT-Battelle, LLC, for the
U.S. Department of Energy under contract DE-AC05-00OR22725.

References

- Antonelli, L., Briani, M., D'Ambra, P., and Fraioli, V.: Positivity Issues in Adaptive Solutions of Detailed
825 Chemical Schemes for Engine Simulations, in: Communications to SIMAI Congress, vol. 3, pp. 303.1–
303.12, 2009.
- Bethke, C. M.: Geochemical and biogeochemical reaction modeling, Cambridge University Press, 2007.
- Bonan, G. B., Hartman, M. D., Parton, W. J., and Wieder, W. R.: Evaluating litter decomposition in earth
830 system models with long-term litterbag experiments: an example using the Community Land Model ver-
sion 4 (CLM4), Global Change Biology, pp. 957–974, doi:10.1111/gcb.12031, <http://dx.doi.org/10.1111/gcb.12031>, 2012.
- Boyer, E. W., Alexander, R. B., Parton, W. J., Li, C., Butterbach-Bahl, K., Donner, S. D., Skaggs, R. W.,
and Grosso, S. J. D.: Modeling Denitrification In Terrestrial And Aquatic Ecosystems At Regional
Scales, Ecological Applications, 16, 2123–2142, doi:10.1890/1051-0761(2006)016, [http://dx.doi.org/10.1890/1051-0761\(2006\)016](http://dx.doi.org/10.1890/1051-0761(2006)016), 2006.
835
- Broekhuizen, N., Rickard, G. J., Bruggeman, J., and Meister, A.: An improved and generalized second order,
unconditionally positive, mass conserving integration scheme for biochemical systems, Applied Numer-
ical Mathematics, 58, 319–340, doi:10.1016/j.apnum.2006.12.002, <http://www.sciencedirect.com/science/article/pii/S0168927406002224>, 2008.
- Bruggeman, J., Burchard, H., Kooi, B. W., and Sommeijer, B.: A second-order, unconditionally
positive, mass-conserving integration scheme for biochemical systems, Applied Numerical Math-
ematics, 57, 36–58, doi:10.1016/j.apnum.2005.12.001, <http://www.sciencedirect.com/science/article/pii/S0168927405002242>, 2007.
840
- Burchard, H., Deleersnijder, E., and Meister, A.: A high-order conservative Patankar-type dis-
cretisation for stiff systems of production–destruction equations, Applied Numerical Mathemat-
ics, 47, 1–30, doi:10.1016/S0168-9274(03)00101-6, <http://www.sciencedirect.com/science/article/pii/S0168927403001016>, 2003.
845
- Burchard, H., Deleersnijder, E., and Meister, A.: Application of modified Patankar schemes to stiff bioge-
chemical models for the water column, Ocean Dynamics, 55, 326–337, doi:10.1007/s10236-005-0001-x,
850 <http://link.springer.com/article/10.1007%2Fs10236-005-0001-x>, 2005.
- Chapin, F., Matson, P., and Vitousek, P.: Principles of Terrestrial Ecosystem Ecology, Springer, 2011.
- Chen, D. and Plemmons, R. J.: Nonnegativity constraints in numerical analysis, in: Symposium on the Birth of
Numerical Analysis, pp. 109–140, 2009.
- da Costa, A. C. L., Galbraith, D., Almeida, S., Portela, B. T. T., da Costa, M., de Athaydes Silva Junior, J.,
855 Braga, A. P., de Gonçalves, P. H. L., de Oliveira, A. A. R., Fisher, R., Phillips, O. L., Metcalfe, D. B., Levy,
P., and Meir, P.: Effect of 7 yr of experimental drought on vegetation dynamics and biomass storage of
an eastern Amazonian rainforest, New Phytologist, 187, 579–591, doi:10.1111/j.1469-8137.2010.03309.x,
<http://dx.doi.org/10.1111/j.1469-8137.2010.03309.x>, 2010.
- Dickinson, R. E., Berry, J. A., Bonan, G. B., Collatz, G. J., Field, C. B., Fung, I. Y., Goulden, M., Hoffmann,
860 W. A., Jackson, R. B., Myneni, R., Sellers, P. J., and Shaikh, M.: Nitrogen Controls on Climate Model
Evapotranspiration, Journal of Climate, 15, 278–295, doi:10.1175/1520-0442(2002)015, [http://dx.doi.org/10.1175/1520-0442\(2002\)015](http://dx.doi.org/10.1175/1520-0442(2002)015), 2002.

- El trop, L. and Marschner, H.: Growth and mineral nutrition of non-mycorrhizal and mycorrhizal Norway spruce (*Picea abies*) seedlings grown in semi-hydroponic sand culture, *New Phytologist*, 133, 469–478, 865 doi:10.1111/j.1469-8137.1996.tb01914.x, <http://dx.doi.org/10.1111/j.1469-8137.1996.tb01914.x>, 1996.
- Falkengren-Grerup, U.: Interspecies differences in the preference of ammonium and nitrate in vascular plants, *Oecologia*, 102, 305–311, doi:10.1007/BF00329797, <http://dx.doi.org/10.1007/BF00329797>, 1995.
- Fang, Y., Huang, M., Liu, C., Li, H., and Leung, L. R.: A generic biogeochemical module for Earth system models: Next Generation BioGeoChemical Module (NGBGC), version 1.0, *Geosci. Model Dev.*, 6, 1977–870 1988, doi:10.5194/gmd-6-1977-2013, <http://www.geosci-model-dev.net/6/1977/2013>, gMD, 2013.
- Fennell, D. E. and Gossett, J. M.: Modeling the Production of and Competition for Hydrogen in a Dechlorinating Culture, *Environmental Science & Technology*, 32, 2450–2460, doi:10.1021/es980136l, <http://pubs.acs.org/doi/pdfplus/10.1021/es980136l>, 1998.
- Foulland, E., Gosselin, M., Rivkin, R. B., Vasseur, C., and Mostajir, B.: Nitrogen uptake by heterotrophic 875 bacteria and phytoplankton in Arctic surface waters, *Journal of Plankton Research*, 29, 369–376, <http://plankt.oxfordjournals.org/content/29/4/369.abstract>, 2007.
- Gherardi, L. A., Sala, O. E., and Yahdjian, L.: Preference for different inorganic nitrogen forms among plant functional types and species of the Patagonian steppe, *Oecologia*, 173, 1075–1081, doi:10.1007/s00442-013-2687-7, <http://dx.doi.org/10.1007/s00442-013-2687-7>, 2013.
- Grant, R. F.: Modelling changes in nitrogen cycling to sustain increases in forest productivity under elevated atmospheric CO₂ and contrasting site conditions, *Biogeosciences*, 10, 7703–7721, doi:10.5194/bg-10-7703-880 2013, <http://www.biogeosciences.net/10/7703/2013>, bG, 2013.
- Gu, C. and Riley, W. J.: Combined effects of short term rainfall patterns and soil texture on soil nitrogen cycling — A modeling analysis, *Journal of Contaminant Hydrology*, 112, 141–154, 885 doi:10.1016/j.jconhyd.2009.12.003, <http://www.sciencedirect.com/science/article/pii/S0169772209001648>, 2010.
- Hammond, G. E.: Innovative Methods for Solving Multicomponent Biogeochemical groundwater Transport on Supercomputers, Thesis, University of Illinois at Urbana-Champaign, 2003.
- Hanson, P. and Wullschleger, S.: North American Temperate Deciduous Forest Responses to Changing Precipitation Regimes, Springer Verlag, 2003.
- Hanson, P. J., Amthor, J. S., Wullschleger, S. D., Wilson, K. B., Grant, R. F., Hartley, A., Hui, D., Hunt, J. E. R., Johnson, D. W., Kimball, J. S., King, A. W., Luo, Y., McNulty, S. G., Sun, G., Thornton, P. E., Wang, S., Williams, M., Baldocchi, D. D., and Cushman, R. M.: Oak forest carbon and water simulations: model intercomparisons and evaluations against independent data, *Ecological Monographs*, 74, 443–489, 895 doi:10.1890/03-4049, <http://www.esajournals.org/doi/pdf/10.1890/03-4049>, 2004.
- Hinkel, K. M. and Nelson, F. E.: Spatial and temporal patterns of active layer thickness at Circumpolar Active Layer Monitoring (CALM) sites in northern Alaska, 1995–2000, *Journal of Geophysical Research: Atmospheres*, 108, 8168, doi:10.1029/2001JD000927, <http://dx.doi.org/10.1029/2001JD000927>, 2003.
- Hungate, R.: The rumen microbial ecosystem, *Annual Review of Ecology and Systematics*, pp. 39–66, 1975.
- HØGh-Jensen, H., Wollenweber, B., and Schjoerring, J. K.: Kinetics of nitrate and ammonium absorption and accompanying H⁺ fluxes in roots of *Lolium perenne* L. and N₂-fixing *Trifolium repens* L, *Plant, Cell & Envi-*

- ronment, 20, 1184–1192, doi:10.1046/j.1365-3040.1997.d01-145.x, <http://dx.doi.org/10.1046/j.1365-3040.1997.d01-145.x>, 1997.
- IPCC: Climate Change 2013: The Physical Science Basis. Contribution of Working Group I to the Fifth Assessment Report of the Intergovernmental Panel on Climate Change, Cambridge University Press, Cambridge, United Kingdom and New York, NY, USA, doi:10.1017/CBO9781107415324, www.climatechange2013.org, 2013.
- Jarrell, K. F.: Extreme Oxygen Sensitivity in Methanogenic Archaeabacteria, *BioScience*, 35, 298–302, <http://bioscience.oxfordjournals.org/content/35/5/298.abstract>, 1985.
- Kamer, K., Kennison, R. L., and Fong, P.: Rates of inorganic nitrogen uptake by the estuarine green macroalgae *Enteromorpha intestinalis* and *Ulva expansa*, vol. 2003, pp. 130–141, 2001.
- Kirchman, D. L.: The uptake of inorganic nutrients by heterotrophic bacteria, *Microbial Ecology*, 28, 255–271, doi:10.1007/BF00166816, <http://dx.doi.org/10.1007/BF00166816>, 1994.
- Kirchman, D. L. and Wheeler, P. A.: Uptake of ammonium and nitrate by heterotrophic bacteria and phytoplankton in the sub-Arctic Pacific, *Deep Sea Research Part I: Oceanographic Research Papers*, 45, 347–365, doi:10.1016/S0967-0637(97)00075-7, <http://www.sciencedirect.com/science/article/pii/S0967063797000757>, 1998.
- Kuzyakov, Y. and Xu, X.: Competition between roots and microorganisms for nitrogen: mechanisms and ecological relevance, *New Phytologist*, 198, 656–669, doi:10.1111/nph.12235, <http://dx.doi.org/10.1111/nph.12235>, 2013.
- Lara, M. J., Villarreal, S., Johnson, D. R., Hollister, R. D., Webber, P. J., and Tweedie, C. E.: Estimated change in tundra ecosystem function near Barrow, Alaska between 1972 and 2010, *Environmental Research Letters*, 7, 015 507, 2012.
- Lichtner, P. C., Hammond, G. E., Lu, C., Karra, S., Bisht, G., Andre, B., Mills, R. T., and Jitu, K.: PFLO-TRAN User Manual: A Massively Parallel Reactive Flow and Transport Model for Describing Surface and Subsurface Processes, Report, 2015.
- Maggi, F., Gu, C., Riley, W. J., Hornberger, G. M., Venterea, R. T., Xu, T., Spycher, N., Steefel, C., Miller, N. L., and Oldenburg, C. M.: A mechanistic treatment of the dominant soil nitrogen cycling processes: Model development, testing, and application, *Journal of Geophysical Research: Biogeosciences*, 113, G02 016, doi:10.1029/2007JG000578, <http://dx.doi.org/10.1029/2007JG000578>, 2008.
- Manzoni, S. and Porporato, A.: Soil carbon and nitrogen mineralization: Theory and models across scales, *Soil Biology and Biochemistry*, 41, 1355–1379, doi:10.1016/j.soilbio.2009.02.031, <http://www.sciencedirect.com/science/article/pii/S0038071709000765>, 2009.
- Middelburg, J. J. and Nieuwenhuize, J.: Nitrogen uptake by heterotrophic bacteria and phytoplankton in the nitrate-rich Thames estuary, *Marine Ecology Progress Series*, 203, 13–21, <http://www.int-res.com/abstracts/meps/v203/p13-21/>, 2000.
- Nollet, L. M. L. and De Gelder, L. S. P.: Handbook of Water Analysis (3rd Edition), CRC Press, 2013.
- Nordin, A., Högberg, P., and Näsholm, T.: Soil nitrogen form and plant nitrogen uptake along a boreal forest productivity gradient, *Oecologia*, 129, 125–132, doi:10.1007/s004420100698, <http://dx.doi.org/10.1007/s004420100698>, 2001.

- Oleson, K., Lawrence, D., Bonan, G., Levis, S., Swenson, S., Thornton, P., Bozbayik, A., Fisher, R., Heald, C., Kluzek, E., Lamarque, J.-F., Lawrence, P., Lipscomb, W., Muszala, S., and Sacks, W.: Technical description of version 4.5 of the Community Land Model (CLM), Ncar/tn-503+str, ncar technical note, NCAR, doi:10.5065/D6RR1W7M, http://www.cesm.ucar.edu/models/cesm1.2/clm/CLM45_Tech_Note.pdf, 2013.
- 945 Parkhurst, D. L. and Appelo, C.: User's guide to PHREEQC (Version 2): A computer program for speciation, batch-reaction, one-dimensional transport, and inverse geochemical calculations, Water-Resources Investigations 99-4259, USGS, 1999.
- Parton, W. J., Mosier, A. R., Ojima, D. S., Valentine, D. W., Schimel, D. S., Weier, K., and Kulmala, A. E.: Generalized model for N₂ and N₂O production from nitrification and denitrification, Global Biogeochemical 950 Cycles, 10, 401–412, doi:10.1029/96GB01455, <http://dx.doi.org/10.1029/96GB01455>, 1996.
- Parton, W. J., Holland, E. A., Del Gross, S. J., Hartman, M. D., Martin, R. E., Mosier, A. R., Ojima, D. S., and Schimel, D. S.: Generalized model for NO_x and N₂O emissions from soils, Journal of Geophysical Research: Atmospheres, 106, 17 403–17 419, doi:10.1029/2001JD900101, <http://dx.doi.org/10.1029/2001JD900101>, 2001.
- 955 Pfautsch, S., Rennenberg, H., Bell, T. L., and Adams, M. A.: Nitrogen uptake by Eucalyptus regnans and Acacia spp. – preferences, resource overlap and energetic costs, Tree Physiology, 29, 389–399, <http://treephys.oxfordjournals.org/content/29/3/389.abstract>, 2009.
- Pierre, M. and Schmitt, D.: Blowup in Reaction-Diffusion Systems with Dissipation of Mass, SIAM Review, 42, 93–106, doi:10.1137/S0036144599359735, <http://dx.doi.org/10.1137/S0036144599359735><http://epubs.siam.org/doi/abs/10.1137/S0036144599359735>, 2000.
- 960 Powell, T. L., Galbraith, D. R., Christoffersen, B. O., Harper, A., Imbuzeiro, H. M. A., Rowland, L., Almeida, S., Brando, P. M., da Costa, A. C. L., Costa, M. H., Levine, N. M., Malhi, Y., Saleska, S. R., Sotta, E., Williams, M., Meir, P., and Moorcroft, P. R.: Confronting model predictions of carbon fluxes with measurements of Amazon forests subjected to experimental drought, New Phytologist, 200, 350–365, doi:10.1111/nph.12390, <http://dx.doi.org/10.1111/nph.12390>, 2013.
- 965 Riley, W. J., Maggi, F., Kleber, M., Torn, M. S., Tang, J. Y., Dwivedi, D., and Guerry, N.: Long residence times of rapidly decomposable soil organic matter: application of a multi-phase, multi-component, and vertically resolved model (BAMS1) to soil carbon dynamics, Geosci. Model Dev., 7, 1335–1355, doi:10.5194/gmd-7-1335-2014, <http://www.geosci-model-dev.net/7/1335/2014/>, gMD, 2014.
- 970 Schmidt, M. W. I., Torn, M. S., Abiven, S., Dittmar, T., Guggenberger, G., Janssens, I. A., Kleber, M., Kogel-Knabner, I., Lehmann, J., Manning, D. A. C., Nannipieri, P., Rasse, D. P., Weiner, S., and Trumbore, S. E.: Persistence of soil organic matter as an ecosystem property, Nature, 478, 49–56, <http://dx.doi.org/10.1038/nature10386>, 10.1038/nature10386, 2011.
- Sellers, P. J., Dickinson, R. E., Randall, D. A., Betts, A. K., Hall, F. G., Berry, J. A., Collatz, G. J., Denning, 975 A. S., Mooney, H. A., Nobre, C. A., Sato, N., Field, C. B., and Henderson-Sellers, A.: Modeling the Exchanges of Energy, Water, and Carbon Between Continents and the Atmosphere, Science, 275, 502–509, doi:10.1126/science.275.5299.502, <http://www.sciencemag.org/content/275/5299/502.abstract>, 1997.
- Seneviratne, S. I., Corti, T., Davin, E. L., Hirschi, M., Jaeger, E. B., Lehner, I., Orlowsky, B., and Teuling, A. J.: Investigating soil moisture–climate interactions in a changing climate: A review, Earth-Science Re-

- 980 views, 99, 125–161, doi:10.1016/j.earscirev.2010.02.004, <http://www.sciencedirect.com/science/article/pii/S0012825210000139>, 2010.
- Shampine, L. F., Thompson, S., Kierzenka, J. A., and Byrne, G. D.: Non-negative solutions of ODEs, Applied Mathematics and Computation, 170, 556–569, doi:<http://dx.doi.org/10.1016/j.amc.2004.12.011>, <http://www.sciencedirect.com/science/article/pii/S0096300304009683>, 2005.
- 985 Steefel, C. I., Appelo, C. A. J., Arora, B., Jacques, D., Kalbacher, T., Kolditz, O., Lagneau, V., Lichtner, P. C., Mayer, K. U., Meeussen, J. C. L., Molins, S., Moulton, D., Shao, H., Šimůnek, J., Spycher, N., Yabusaki, S. B., and Yeh, G. T.: Reactive transport codes for subsurface environmental simulation, Computational Geosciences, pp. 1–34, doi:10.1007/s10596-014-9443-x, <http://dx.doi.org/10.1007/s10596-014-9443-x>, 2014.
- Tang, G., Watson, D. B., Wu, W.-M., Schadt, C. W., Parker, J. C., and Brooks, S. C.: U(VI) Bioreduction with 990 Emulsified Vegetable Oil as the Electron Donor – Model Application to a Field Test, Environmental Science & Technology, 47, 3218–3225, doi:10.1021/es304643h, <http://dx.doi.org/10.1021/es304643h>, 2013a.
- Tang, J., Riley, W., Koven, C., and Subin, Z.: CLM4-BeTR, a generic biogeochemical transport and reaction module for CLM4: model development, evaluation, and application, Geoscientific Model Development, 6, 127–140, 2013b.
- 995 Thornton, P. E. and Rosenbloom, N. A.: Ecosystem model spin-up: Estimating steady state conditions in a coupled terrestrial carbon and nitrogen cycle model, Ecological Modelling, 189, 25–48, doi:10.1016/j.ecolmodel.2005.04.008, <http://www.sciencedirect.com/science/article/pii/S0304380005001948>, 2005.
- Veuger, B., Middelburg, J. J., Boschker, H. T. S., Nieuwenhuize, J., van Rijswijk, P., Rochelle-Newall, E. J., 1000 and Navarro, N.: Microbial uptake of dissolved organic and inorganic nitrogen in Randers Fjord, Estuarine, Coastal and Shelf Science, 61, 507–515, doi:10.1016/j.ecss.2004.06.014, <http://www.sciencedirect.com/science/article/pii/S0272771404001593>, 2004.
- Wang, G., Post, W. M., and Mayes, M. A.: Development of microbial-enzyme-mediated decomposition model parameters through steady-state and dynamic analyses, Ecological Applications, 23, 1005 255–272, doi:10.1890/12-0681.1, <http://dx.doi.org/10.1890/12-0681.1><http://www.esajournals.org/doi/abs/10.1890/12-0681.1>, 2012.
- Warren, C. R. and Adams, P. R.: Uptake of nitrate, ammonium and glycine by plants of Tasmanian wet eucalypt forests, Tree Physiology, 27, 413–419, <http://treephys.oxfordjournals.org/content/27/3/413.abstract>, doi:10.1093/treephys/27.3.413, 2007.
- 1010 Xu, T., Sonnenthal, E., Spycher, N., and Pruess, K.: TOUGHREACT—A simulation program for non-isothermal multiphase reactive geochemical transport in variably saturated geologic media: Applications to geothermal injectivity and CO₂ geological sequestration, Computers & Geosciences, 32, 145–165, doi:10.1016/j.cageo.2005.06.014, <http://www.sciencedirect.com/science/article/pii/S0098300405001500>, 2006.

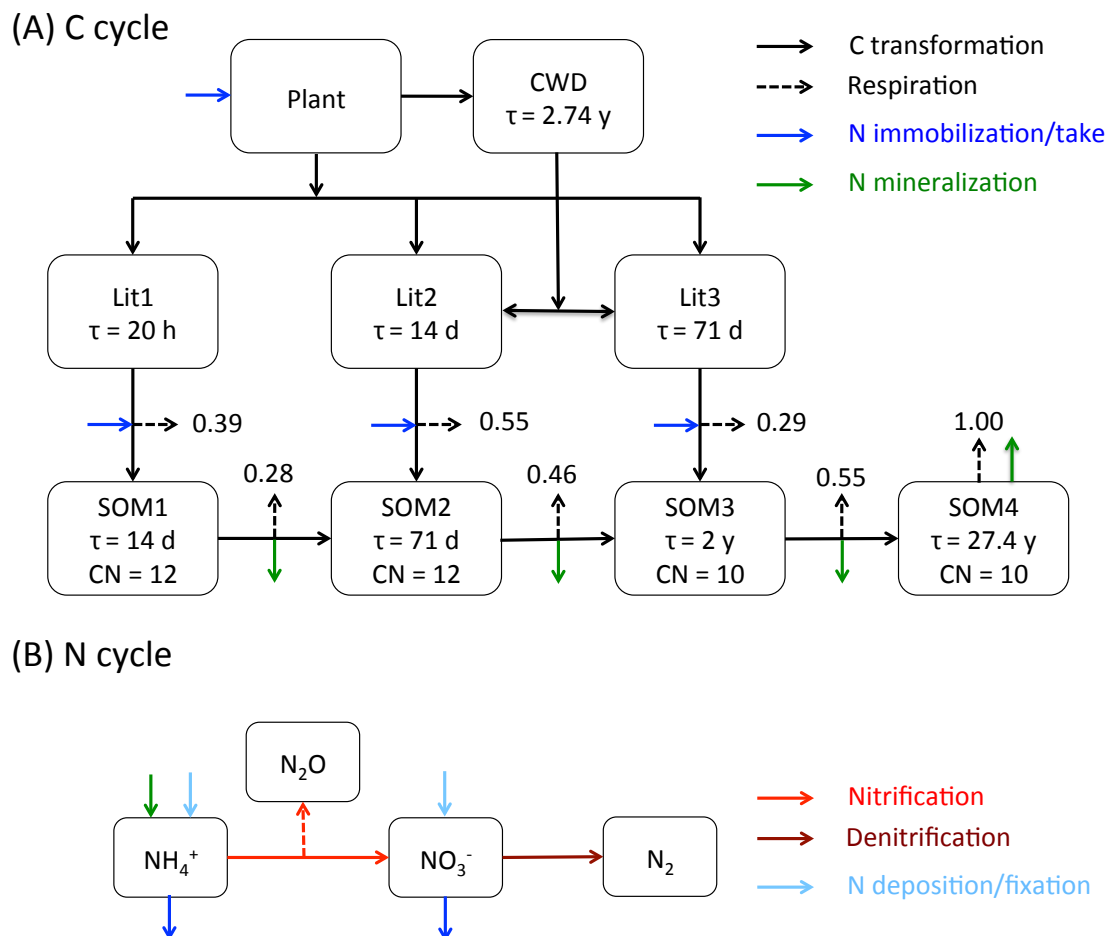


Figure 1. The reaction network for the carbon (A) and nitrogen (B) cycles implemented in this work. The carbon cycle is modified from Thornton and Rosenbloom (2005) and Bonan et al. (2012)

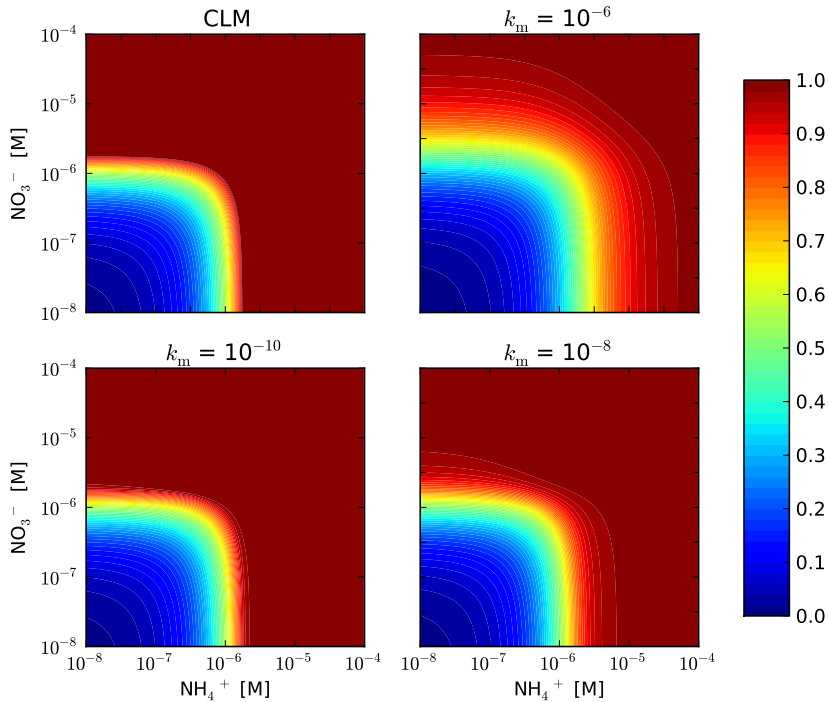


Figure 2. The ratio of uptake and demand (f_{pi} in Eq. 29) as a function of concentrations with CLM and representation by Eqs. (27) and (28) in a 0.5 h time step with an uptake rate of 10^{-9} M s^{-1} . f_{pi} for the new representation is less than or equal to that for CLM. The difference decreases with decreasing half saturation k_m .

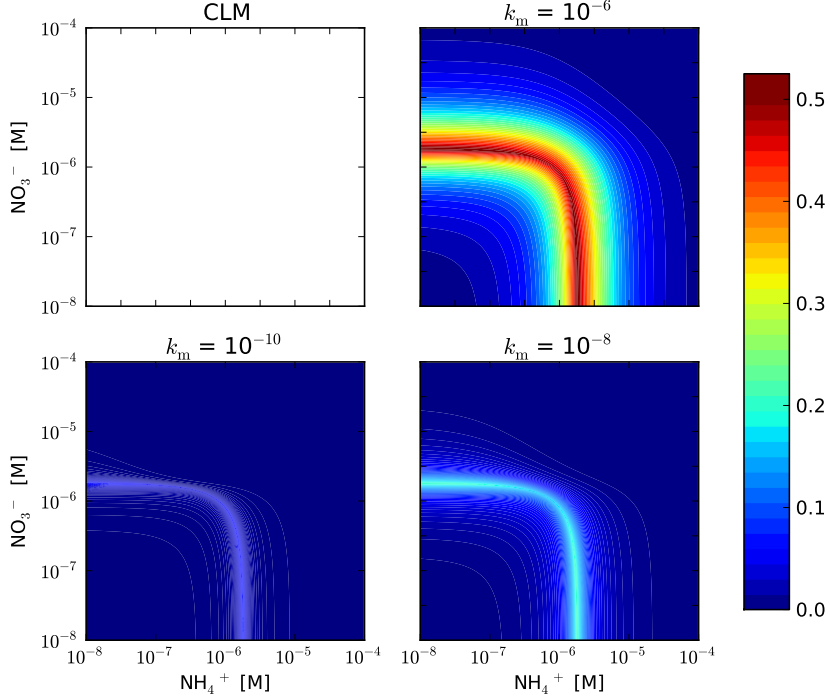


Figure 3. The difference plots for Fig. (2).

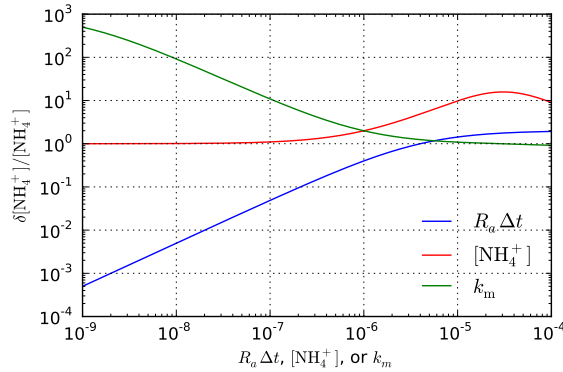


Figure 4. The calculated ratio of update over concentration for the first iteration as a function of time step size ($R_a \Delta t$), initial concentration (NH_4^+), and half saturation (k_m) for solving $d[\text{NH}_4^+]/dt = -R_a[\text{NH}_4^+]/(\text{NH}_4^+ + k_m)$ using the backward Euler method and Newton-Raphson method. Without scaling back the update (δ), the concentration in the first iteration step ($[\text{NH}_4^+]^{k+1,1}$) can go negative if $R_a \Delta t > 10^{-5}$, $[\text{NH}_4^+]^k > 10^{-6}$, or $k_m < 10^{-6}$. Unless specified in the figure, the base case parameters are $R_a \Delta t = 10^{-3}$, $\text{NH}_4^+ = 10^{-6}$, and $k_m = 10^{-6}$.

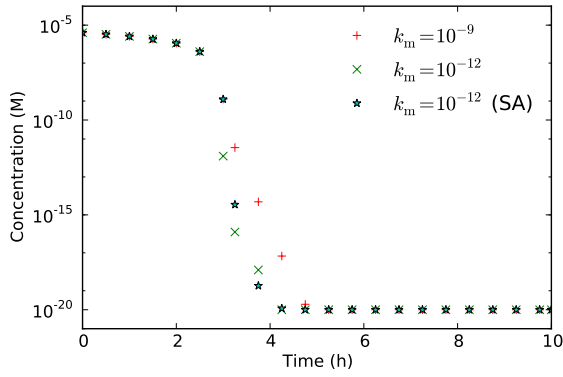


Figure 5. Influence of half saturation (k_m) on the simulated NH_4^+ concentration decrease due to plant uptake. Too small a half saturation may result in false convergence due to too small an update (scaling factor) during the iteration. The semi-analytical (SA) solution (Eq. 34) is used for comparison.

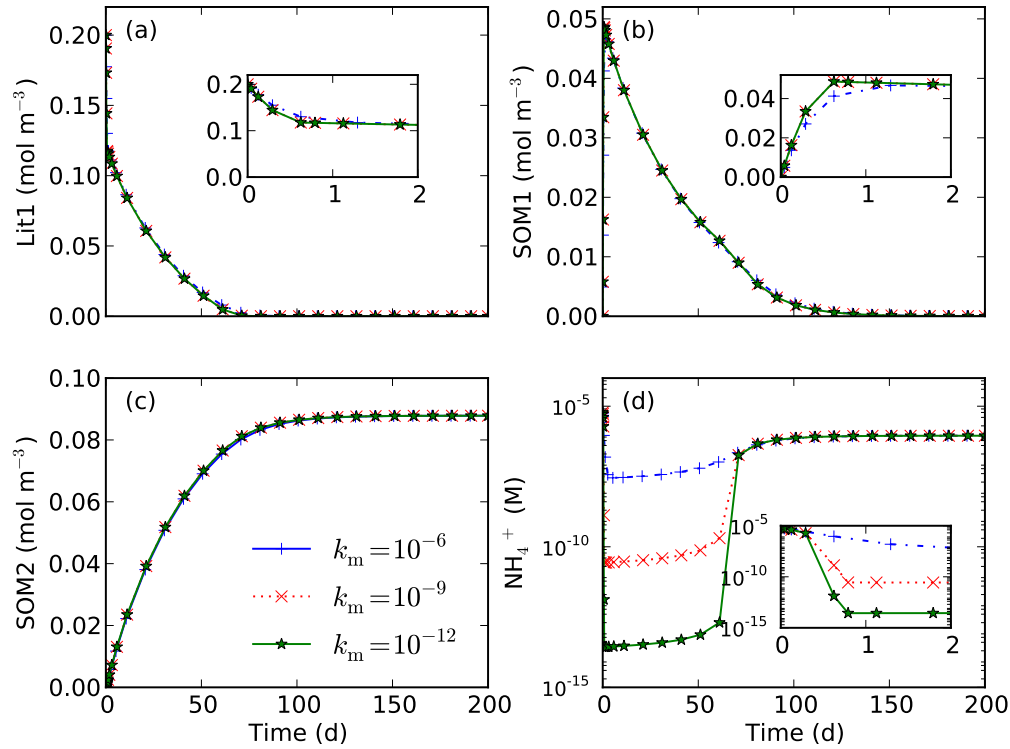


Figure 6. Influence of half saturation k_m on decomposition that involves both nitrogen immobilization and mineralization. Smaller half saturation can result in lower nitrogen concentration (d) but does not substantially impact the calculated concentrations other than NH_4^+ (a,b,c).

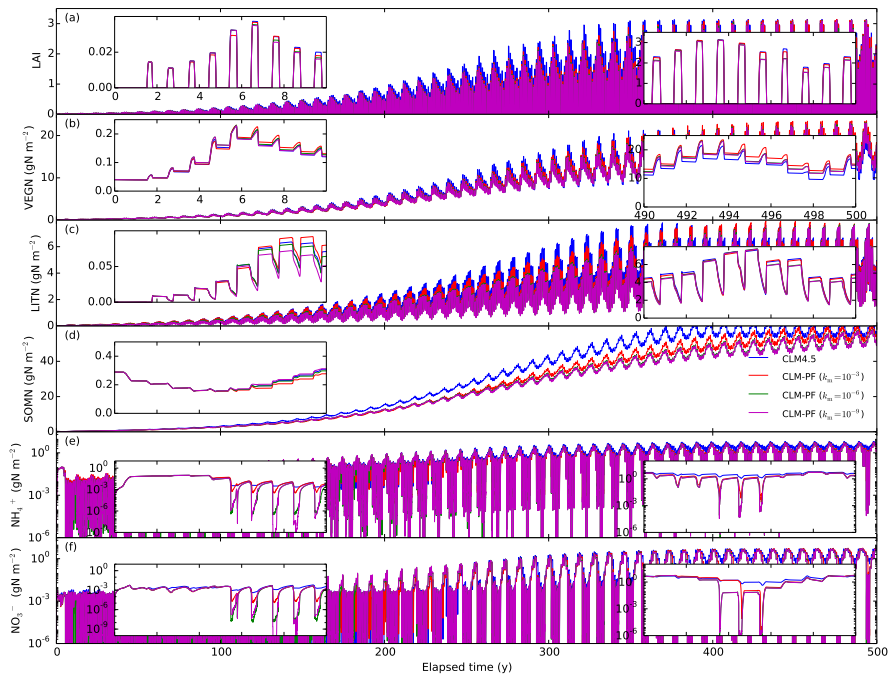


Figure 7. Calculated LAI and nitrogen distribution among vegetation, litter, SOM, NH_4^+ , and NO_3^- pools in spin-up simulations for the US-Brw site. Log transformation is used to enforce nonnegativity for CLM-PFLTRAN.

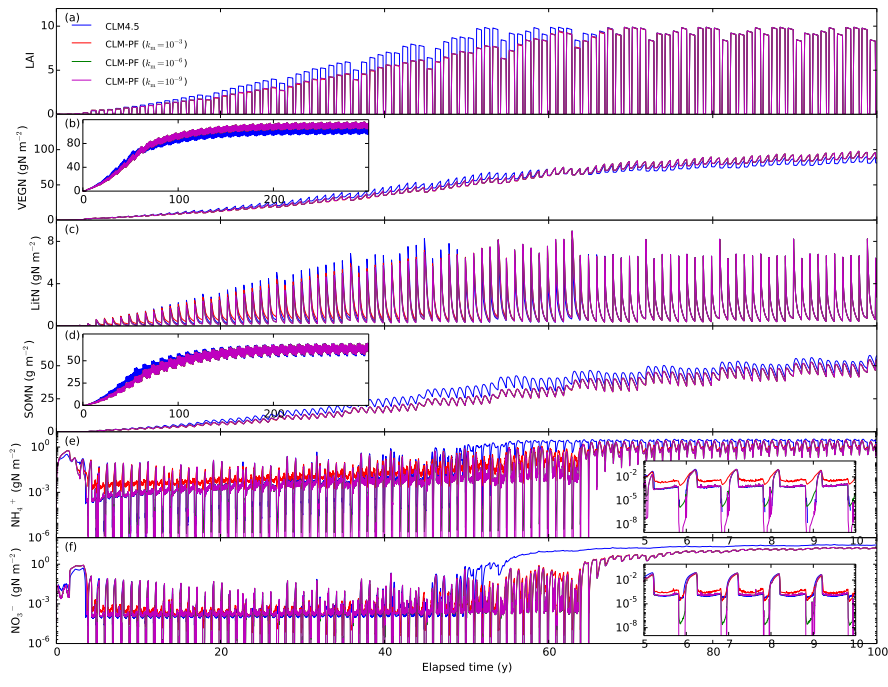


Figure 8. Calculated LAI and nitrogen distribution among vegetation, litter, SOM, NH_4^+ , and NO_3^- pools in spin-up simulations for US-WBW site. Log transformation is used to enforce nonnegativity for CLM-PFLTRAN calculations.

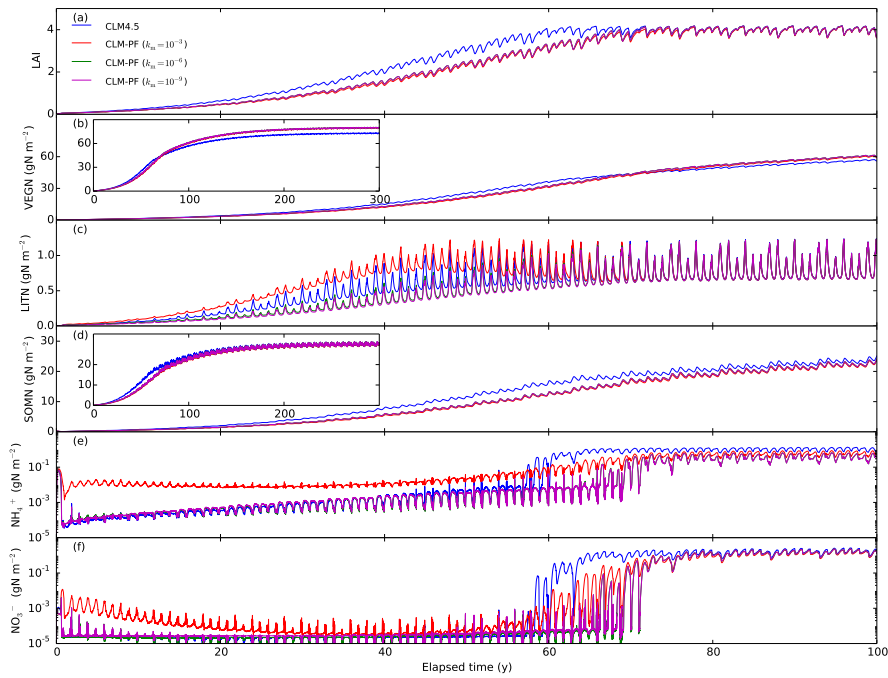


Figure 9. Calculated LAI and nitrogen distribution among vegetation, litter, SOM, NH_4^+ , and NO_3^- pools in spin-up simulations for BR-Cax site. Log transformation is used to enforce nonnegativity for CLM-PFLOTRAN calculations.

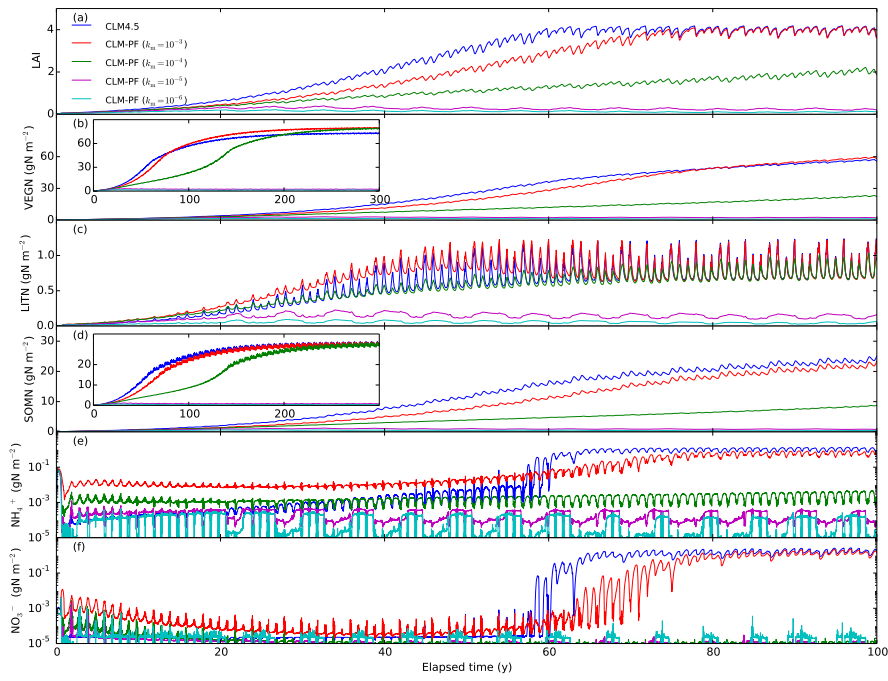


Figure 10. Calculated LAI and nitrogen distribution among vegetation, litter, SOM, NH_4^+ , and NO_3^- pools in spin-up simulations for BR-Cax site. Scaling back update in each iteration is used enforce nonnegativity for CLM-PFLOTTRAN.

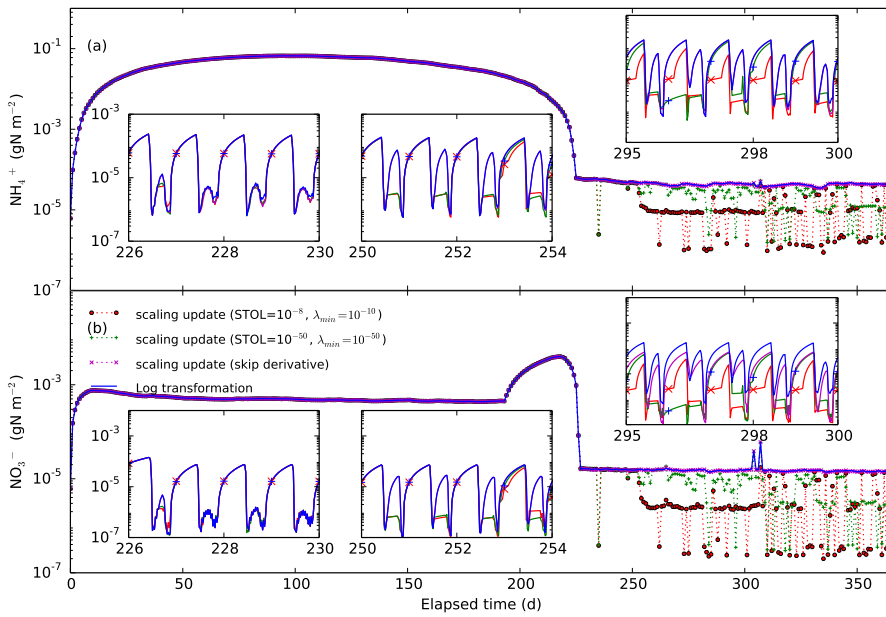


Figure 11. Calculated NH_4^+ and NO_3^- concentration in the first year using SU (scaling update) vs. LT (log transformation) in the spin-up simulation for BR-Cax site with $k_m = 10^{-6} \text{ mol m}^{-3}$. “skip derivative” refers to not including the derivatives for the reaction (R11) with rate (Eq. 30) in the entries for N_2Od in the Jacobian matrix.

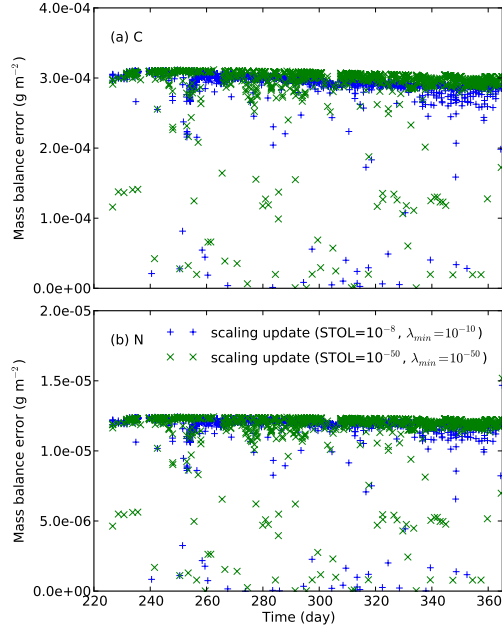


Figure 12. Mass balance error for (a) C and (b) N in the first year where SU with $k_m = 10^{-6}$ mol m⁻³ is used for the tropical site.

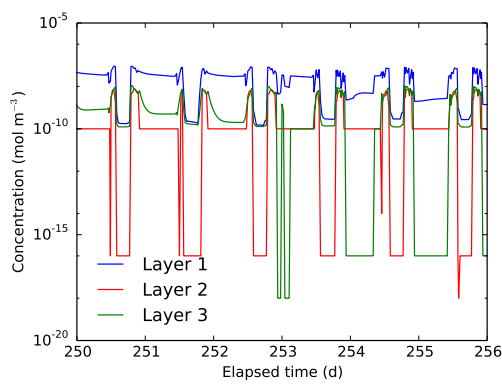


Figure 13. Diagnostic N₂O concentration (N₂Od from nitrification associated with net nitrogen mineralization Reaction R11 and rate Eq. A5) in the spin-up simulation for the BR-Cax site with $k_m = 10^{-6}$ mol m⁻³. The concentration is reset to 10^{-10} at the beginning of each CLM half hour time step. Scaling back update in each iteration is used to enforce nonnegativity.

Table 1. Iterations in solving $dc/dt = -R_a c/(c + k_m)$ using backward Euler method and Newton-Raphson method for one time step $R_a \Delta t = 0.001$ with initial $c = 10^{-3}$ and $k_m = 10^{-6}$

Iteration	c	$c/(k_m+c)$	$s/(c+k_m)^2$	Residual	Jacobian	δ
1	0.001	9.99E-01	9.98E-01	9.99E-01	1.00E+03	0.000998005
2	1.99501E-06	6.66E-01	1.11E+05	-3.32E-01	1.12E+05	-2.95065E-06
3	4.94566E-06	8.32E-01	2.83E+04	-1.63E-01	2.93E+04	-5.57379E-06
4	1.05195E-05	9.13E-01	7.54E+03	-7.63E-02	8.54E+03	-8.93755E-06
5	1.9457E-05	9.51E-01	2.39E+03	-2.94E-02	3.39E+03	-8.68139E-06
6	2.81384E-05	9.66E-01	1.18E+03	-6.18E-03	2.18E+03	-2.838E-06
7	3.09764E-05	9.69E-01	9.78E+02	-2.97E-04	1.98E+03	-1.49981E-07
8	3.11264E-05	9.69E-01	9.69E+02	-6.85E-07	1.97E+03	-3.47801E-10
9	3.11267E-05	9.69E-01	9.69E+02	-3.65E-12	1.97E+03	-1.85288E-15
10	3.11267E-05	9.69E-01	9.69E+02	0	1.97E+03	0

Table 2. Iterations in solving $dc/dt = -R_a c/(c + k_m)$ using backward Euler method and Newton-Raphson method for one time step $R_a \Delta t = 0.002$ with initial $c = 10^{-3}$ and $k_m = 10^{-6}$ (without scaling back δ)

Iteration	c	$c/(k_m+c)$	$s/(c+k_m)^2$	Residual	Jacobian	δ
1	0.001	9.99E-01	9.98E-01	9.99E-01	5.01E+02	0.001994022
2	-0.000994022	1.00E+00	1.01E+00	4.00E-03	5.01E+02	7.97596E-06
3	-0.001001998	1.00E+00	9.98E-01	6.44E-08	5.01E+02	1.28641E-10
4	-0.001001998	1.00E+00	9.98E-01	0.00E+00	5.01E+02	0

Table 3. Iterations in solving $dc/dt = -R_a c/(c + k_m)$ using backward Euler method and Newton-Raphson method for one time step $R_a \Delta t = 0.002$ with initial $c = 10^{-3}$, $k_m = 10^{-6}$, and $\alpha = 0.9999$ for scaling back δ

Iteration	c	$c/(k_m+c)$	$s/(c+k_m)^2$	Residual	Jacobian	δ	λ
1	0.001	9.99E-01	9.98E-01	9.99E-01	5.01E+02	0.001994022	0.5
2	1E-07	9.09E-02	8.26E+05	-4.09E-01	8.27E+05	-4.9464E-07	1
3	5.9464E-07	3.73E-01	3.93E+05	-1.27E-01	3.94E+05	-3.22036E-07	1
4	9.16676E-07	4.78E-01	2.72E+05	-2.13E-02	2.73E+05	-7.80252E-08	1
5	9.94701E-07	4.99E-01	2.51E+05	-8.31E-04	2.52E+05	-3.29904E-09	1
6	9.98001E-07	4.99E-01	2.51E+05	-1.37E-06	2.51E+05	-5.45442E-12	1
7	9.98006E-07	5.00E-01	2.50E+05	-3.73E-12	2.51E+05	-1.48611E-17	1
8	9.98006E-07	5.00E-01	2.50E+05	0	2.51E+05	0	1

Table 4. Iterations in solving $dc/dt = -R_a c/(c + k_m)$ using backward Euler method and Newton-Raphson method for one time step $R_a \Delta t = 0.002$ with initial $c = 10^{-3}$ and $k_m = 10^{-6}$ and with log transformation

Iteration	c	$c/(k_m+c)$	$s/(c+k_m)^2$	Residual	Jacobian	δ
1	0.001	9.99E-01	9.98E-01	9.99E-01	5.01E-01	1.994021918
2	0.000136147	9.93E-01	5.32E+01	5.61E-01	7.53E-02	7.446148992
3	7.94668E-08	7.36E-02	8.58E+05	-4.26E-01	6.82E-02	-6.247977459
4	4.10817E-05	9.76E-01	5.65E+02	4.97E-01	4.37E-02	11.35765187
5	4.79825E-10	4.80E-04	9.99E+05	-5.00E-01	4.80E-04	-1041.52556

Table 5. Wall time (hour) for spin-up simulation at the arctic, temperate, and tropical sites on OIC

Site	CLM	SU (10^{-3})	SU (10^{-6})	SU (10^{-9})	LT (10^{-3})	LT (10^{-6})	LT (10^{-9})	LT (10^{-12})
DC								
US-Brw	18.1	24.8	25.5	29.2	38.5	40.8	47.0	49.5
US-Pit	11.7	17.1	14.8	14.9	30.0	37.5	40.2	43.1
BR-Cax	10.9	16.2	18.6	18.0	40.2	40.5	45.7	52.0
DR								
US-Brw	18.1	21.5	21.5		35.8	35.9		
US-Pit	11.7	14.1	14.1		26.9	26.7		
BR-Cax	10.9	16.4	16.4		42.2	41.6		

SU = scaling update, LT = log transformation, 10^{-3} , 10^{-6} , and 10^{-9} are k_m , DC and DR = downregulating consumption as a function of concentration and rate, OIC = ORNL Institutional Cluster (Phase5), US-Brw simulation duration = 500 year and US-Pit and BR-Cax simulation duration = 300 year. For the last column LT (10^{-12}), MAX_CUT is increased from default 16 to 50.

Table 6. CLM-PFLOTRAN simulation termination before conclusion using scaling back update in iteration

Site	k_m	year	species	concentration	update	layer
$STOL = 10^{-8}$						
US-Brw	10^{-12}	346.66	NO_3^-	1.26×10^{-26}	8.20×10^{-15}	4
US-Pit	10^{-12}	3.56	NO_3^-	2.67×10^{-26}	2.49×10^{-14}	8
BR-Cax	10^{-12}	3.18	NO_3^-	2.54×10^{-26}	5.72×10^{-14}	8
$STOL = 10^{-12}$						
US-Brw	10^{-6}	41.78	DeniN	10^{-20}	2.31×10^{-10}	2
US-Brw	10^{-9}	5.56	PlantN	6.68×10^{-18}	8.12×10^{-8}	2
US-PIT	10^{-3}	7.81	N_2Od	10^{-20}	1.74×10^{-9}	1
US-PIT	10^{-6}	2.40	PlantN	10^{-18}	2.30×10^{-6}	1
BR-Cax	10^{-3}	1.59	N_2Od	10^{-20}	1.66×10^{-10}	1
BR-Cax	10^{-6}	0.64	N_2Od	10^{-20}	1.91×10^{-10}	2
BR-Cax	10^{-9}	0.59	PlantN	10^{-18}	4.92×10^{-8}	2

1015 **Appendix A: CLM biogeochemical reactions and rates**

A1 CLM-CN decomposition

The CLM-CN decomposition cascade consists of three litter pools with variable CN ratios, four soil organic matter (SOM) pools with constant CN ratios, and seven reactions (Fig. 1A). The reaction can be described by



with CN_u and CN_d as the upstream and downstream pool (molecular formula, for 1 mol upstream and downstream pool, there is u and d mol N), N as either NH_4^+ or NO_3^- , f as the respiration fraction, and $n = u - (1 - f)d$. The rate is

$$\frac{d[\text{CN}_u]}{dt} = -k_d f_T f_w [\text{CN}_u], \quad (\text{A1})$$

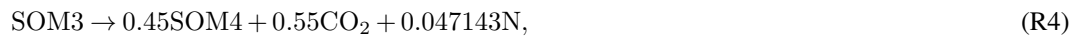
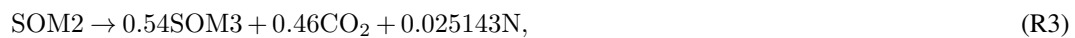
1025 with k_d as the rate coefficient and f_T and f_w as the temperature and moisture response functions,

$$f_T = Q_{10}^{(T-25)/10}, \quad (\text{A2})$$

and

$$f_w = \ln(\psi) Q_{10}^{(T-25)/10}, \quad (\text{A3})$$

With a constant CN ratio, the decomposition reactions for the four SOM pools are



1035 and



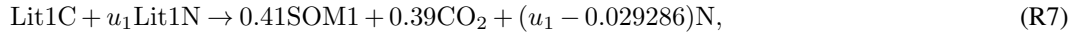
The exact stoichiometric coefficients are calculated in the code using values for respiration factor, CN ratio, and molecular weight specified in the input file.

CLM4.5 has an option to separate N into NH_4^+ and NO_3^- . The N mineralization product is NH_4^+ .

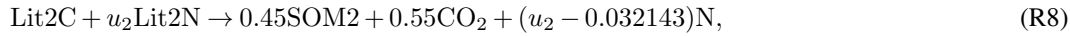
1040 As the CN ratio is variable for the three litter pools, litter N pools need to be tracked such that reaction (R1) becomes



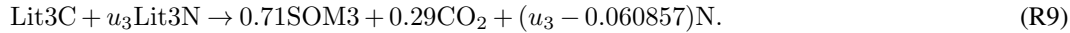
with $u = [\text{LitN}]/[\text{LitC}]$. The three litter decomposition reactions are



1045



and



As the CN ratio of the litter pools is generally high, u_1 , u_2 , and u_3 are usually small, and n in these reactions (e.g., $n_1 = u_1 - 0.029286$ for Lit1) is normally negative. Namely, these reactions consume (immobilize) N, which can be NH_4^+ , NO_3^- , or both.

A2 Nitrification

The nitrification reaction to produce NO_3^- is



1055 with \dots for additional reactants and products to balance the reaction. The rate is (Dickinson et al., 2002)

$$\frac{d[\text{NH}_4^+]}{dt} = -\frac{d[\text{NO}_3^-]}{dt} = -k_n f_T f_w [\text{NH}_4^+]. \quad (\text{A4})$$

The nitrification reaction to produce N_2O is



1060 with one component related to decomposition as

$$\frac{d[\text{NH}_4^+]}{dt} = -2 \frac{d[\text{N}_2\text{O}]}{dt} = -f_{nm} f_T f_w f_{pH} \max(R_{nm}, 0) \quad (\text{A5})$$

with f_{nm} as a fraction (Parton et al., 1996) and R_{nm} as the net N mineralization rate,

$$R_{nm} = \sum_i n_i R_i, \quad (\text{A6})$$

where R_i denotes the rate of reaction (R2, R3, R4, R5, R7, R8, R9). The second component is 1065 (Parton et al., 1996)

$$\frac{d[\text{NH}_4^+]}{dt} = -2 \frac{d[\text{N}_2\text{O}]}{dt} = -k_{n2o} f_T f_w f_{pH} (1 - e^{-0.0105[\text{NH}_4^+]}). \quad (\text{A7})$$

Ignoring the high-order terms and moving the unit conversion factor into k_{n2o} , it can be simplified as a first-order rate as

$$\frac{d[\text{NH}_4^+]}{dt} = -2 \frac{d[\text{N}_2\text{O}]}{dt} = -k_{n2o} f_T f_w f_{pH} [\text{NH}_4^+]. \quad (\text{A8})$$

1070 **A3 Denitrification**

The denitrification reaction is



with rate (Dickinson et al., 2002)

$$\frac{d[\text{NO}_3^-]}{dt} = -2\frac{d[\text{N}_2]}{dt} = -k_{\text{deni}} f_T f_w f_{\text{pH}} [\text{NO}_3^-]. \quad (\text{A9})$$

1075 **A4 Plant nitrogen uptake**

The plant nitrogen uptake reaction can be written as



and



- 1080 The rate is specified by CLM (plant nitrogen demand) and assumed to be constant in each half-hour time step.

A5 Demand-based competition and distributing nitrogen demand between NH_4^+ and NO_3^-

Denote $R_{d,p}$, $R_{d,i}$, $R_{d,nitr}$, $R_{d,deni}$ as the potential plant, immobilization, nitrification, and denitrification demand (rate); $R_{a,tot} = R_{d,p} + R_{d,i} + R_{d,nitr}$ as the total NH_4^+ demand; and $R_{n,tot}$ as the total NO_3^- demand. CLM uses a demand-based competition approach to split the available sources in proportion to the demand rates to meet the demands (Oleson et al., 2013; Thornton and Rosenbloom, 2005). Specifically, for each time step, if $R_{a,tot}\Delta t \leq [\text{NH}_4^+]$, the uptakes are equal to potential demands, and $R_{n,tot} = 0$; otherwise, the uptakes for NH_4^+ are $[\text{NH}_4^+]R_{d,p}/R_{a,tot}\Delta t$, $[\text{NH}_4^+]R_{d,i}/R_{a,tot}\Delta t$, and $[\text{NH}_4^+]R_{d,nitr}/R_{a,tot}\Delta t$ for plants, immobilization, and nitrification, respectively; $R_{n,tot} = R_{a,tot} - [\text{NH}_4^+]/\Delta t + R_{d,deni}$. If $R_{n,tot}\Delta t < [\text{NO}_3^-]$, all of the remaining demand $R_{n,tot}$ is met with available NO_3^- . Otherwise, available NO_3^- is split to meet the remaining plant, immobilization, and denitrification demands in proportion to their rates.

Appendix B: Downregulation of consumption as a function of rates

The contribution of n reactions to the rate component in the residual and Jacobian for species i are

$$1095 \quad \mathbf{R}(i) = \sum_{j=1}^n \nu_{ij} R_j, \quad (\text{B1})$$

and

$$\mathbf{J}(i,k) = \frac{\partial \mathbf{R}(i)}{\partial \mathbf{C}(k)} = \sum_{j=1}^n \frac{\partial(\nu_{ij} R_j)}{\partial \mathbf{C}(k)}, \quad (\text{B2})$$

with \mathbf{C} as the concentration vector, \mathbf{R} as the rate vector, \mathbf{J} as the component of Jacobian matrix (m by m) that is associated with \mathbf{R} , ν_{ij} as stoichiometric coefficient of species i in reaction j ($\sum_{i=1}^m \nu_{ij} \mathbf{C}(i) = 0$), and R_j as the rate of reaction j , a function of the activities (concentration) of the reactants, products, and environmental variables (moisture, temperature, pH, redox, etc.).

B1 Downregulation of consumption for one species

Depending on whether a species a (e.g., NH_4^+) is a reactant ($\nu_{aj} > 0$) or a product ($\nu_{aj} < 0$), we divide the n reactions into a demand (subscript da for demand a) and a supply (subscript sa for supply a) group:

$$R_{da} = \sum_{j=1}^{n_{da}} \nu_{da,aj} R_{da,j}, \quad (\text{B3})$$

and

$$R_{sa} = \sum_{j=1}^{n_{sa}} \nu_{sa,aj} R_{sa,j}, \quad (\text{B4})$$

with n_{da} as the number of reactions that consume species a , $\nu_{da,aj}$ as the stoichiometric coefficient of species i in a consuming reaction j , n_{sa} as the number of reactions that produce species a , $\nu_{sa,ij}$ as the stoichiometric coefficient of species i in a producing reaction j , R_{da} as a consumption (demand) rate (mol s^{-1} , negative), and R_{sa} as a production (supply) rate (mol s^{-1} , positive). Therefore,

$$\mathbf{R}(i) = \sum_{j=1}^{n_{sa}} \nu_{sa,aj} R_{sa,j} + \sum_{j=1}^{n_{da}} \nu_{da,aj} R_{da,j} = \mathbf{R}_{sa}(i) + \mathbf{R}_{da}(i), \quad (\text{B5})$$

and

$$\mathbf{J}(i, k) = \frac{\partial \mathbf{R}(i)}{\partial \mathbf{C}(k)} = \sum_{j=1}^n \frac{\partial(\nu_{ij} R_j)}{\partial \mathbf{C}(k)} = \sum_{j=1}^{n_{sa}} \frac{\partial(\nu_{sa,ij} R_{sa,j})}{\partial \mathbf{C}(k)} + \sum_{j=1}^{n_{da}} \frac{\partial(\nu_{da,ij} R_{da,j})}{\partial \mathbf{C}(k)} = \mathbf{J}_{sa} + \mathbf{J}_{da}. \quad (\text{B6})$$

Define a downregulation factor

$$d_a = \min \left(1, -\frac{R_{sa} \Delta t + [\mathbf{C}(a) - \epsilon] V}{R_{da} \Delta t} \right) = \min \left(1, -\frac{s_a}{D_a} \right), \quad (\text{B7})$$

with V as the bulk volume or volume of liquid water of the grid cell for species with concentration unit mol m^{-3} or M. After downregulation,

$$\mathbf{R}_a = \mathbf{R}_{sa} + d_a \mathbf{R}_{da}, \quad (\text{B8})$$

$$\mathbf{J}_a(i, k) = \frac{\partial \mathbf{R}_a(i)}{\partial \mathbf{C}(k)} = \mathbf{J}_{sa}(i, k) + d_a \mathbf{J}_{da}(i, k) + \mathbf{R}_{da}(i) \frac{\partial d_a}{\partial \mathbf{C}(k)}, \quad (\text{B9})$$

$$\frac{\partial d_a}{\partial \mathbf{C}(k)} = - \left(\frac{\partial s_a}{\partial \mathbf{C}(k)} D_a - s_a \frac{\partial D_a}{\partial \mathbf{C}(k)} \right) D_a^{-2}, \quad (\text{B10})$$

$$\frac{\partial s_a}{\partial \mathbf{C}(a)} = \sum_{j=1}^{n_{sa}} \frac{\partial(\nu_{sa,aj} R_{sa,j})}{\partial \mathbf{C}(a)} \Delta t + V, \quad (\text{B11})$$

$$\frac{\partial s_a}{\partial \mathbf{C}(k)} = \sum_{j=1}^{n_{sa}} \frac{\partial(\nu_{sa,kj} R_{sa,j})}{\partial \mathbf{C}(k)} \Delta t, \quad (\text{B12})$$

$$1125 \quad \frac{\partial D_a}{\partial \mathbf{C}(k)} = \sum_{j=1}^{n_{da}} \frac{\partial(\nu_{da,kj} R_{da,j})}{\partial \mathbf{C}(k)} \Delta t, \quad (\text{B13})$$

Implementation in PFLOTRAN involves 1) adding variables \mathbf{R}_{sa} , \mathbf{R}_{da} , and \mathbf{J}_a , 2) accumulating the values in each reaction rate formula, and 3) conducting downregulation and adding the contribution to the global residual vector and Jacobian matrix.

B2 Downregulation of consumption for a second species

- 1130 In addition to species a (e.g., NH_4^+), we want to downregulate another species l , for example, NO_3^- . The treatment is the same except for the reactions that consume species a and produce species l . Suppose we have a nitrification reaction (R10) with rate R_{al} , and $R'_{al} = dR_{al}/d[\text{NH}_4^+]$. The rate and derivative are added in demand rate and derivative for NH_4^+ (\mathbf{R}_{sa} , \mathbf{R}_{da} , \mathbf{J}_{sa} , \mathbf{J}_{da}), not in the sink rate and derivative for NO_3^- (\mathbf{R}_{sl} , \mathbf{R}_{dl} , \mathbf{J}_{sl} , \mathbf{J}_{dl}). Define a downregulation factor

$$1135 \quad d_l = \min \left(1, - \frac{R_{sl} \Delta t + (\mathbf{C}(l) - \epsilon) V_w + \underline{R_{al} d_a \Delta t}}{R_{dl} \Delta t} \right) = \min(1, - \frac{s_l}{D_l}), \quad (\text{B14})$$

$$\mathbf{R}_l = \mathbf{R}_{sl} + d_l \mathbf{R}_{dl}, \quad (\text{B15})$$

$$\mathbf{J}_l(i, k) = \frac{\partial \mathbf{R}_l(i)}{\partial \mathbf{C}(k)} = \mathbf{J}_{sl}(i, k) + d_l \mathbf{J}_{dl}(i, k) + \mathbf{R}_{dl}(i) \frac{\partial d_l}{\partial \mathbf{C}(k)}, \quad (\text{B16})$$

$$\frac{\partial d_l}{\partial \mathbf{C}(k)} = - \left(\frac{\partial s_l}{\partial \mathbf{C}(k)} D_l - s_l \frac{\partial D_l}{\partial \mathbf{C}(k)} \right) D_l^{-2}, \quad (\text{B17})$$

$$\frac{\partial s_l}{\partial \mathbf{C}(l)} = \sum_{j=1}^{n_{sl}} \frac{\partial(\nu_{sl,lj} R_{sl,j})}{\partial \mathbf{C}(l)} \Delta t + V_w + \underline{\frac{\partial(R_{al} d_a)}{\partial \mathbf{C}(l)}}, \quad (\text{B18})$$

1140
$$\frac{\partial s_l}{\partial \mathbf{C}(k)} = \sum_{j=1}^{n_{sl}} \frac{\partial(\nu_{sl,kj} R_{sl,j})}{\partial \mathbf{C}(k)} \Delta t + \underline{\frac{\partial(R_{al} d_a)}{\partial \mathbf{C}(K)}}, \quad (\text{B19})$$

and

$$\frac{\partial D_a}{\partial \mathbf{C}(k)} = \sum_{j=1}^{n_{da}} \frac{\partial(\nu_{da,kj} R_{da,j})}{\partial \mathbf{C}(k)} \Delta t. \quad (\text{B20})$$

In addition to variables \mathbf{R}_{sl} , \mathbf{R}_{dl} , and \mathbf{J}_l , downregulating the second species requires two additional variables, R_{al} , and R'_{al} . When accumulating the values in each reaction rate formula, the 1145 production rate from the reaction that consumes the first species has to be carefully treated as it is downregulated for the first species. Conducting downregulation involves additional terms, as underlined in the equations. Compared with the downregulation for the first species, downregulating the second species that can be produced from the first species with a simple $A \rightarrow B$ reaction becomes much more complicated. If we add another reaction that consumes the second species to produce the 1150 first species, this approach has to be modified.

In general, many if not all species need to be downregulated. Extending this approach involves adding many variables (vectors and matrices) to track the consumption and production rates and their derivatives. The consumption and production relationship among many species can be complicated, making generalization of this approach challenging if not infeasible.

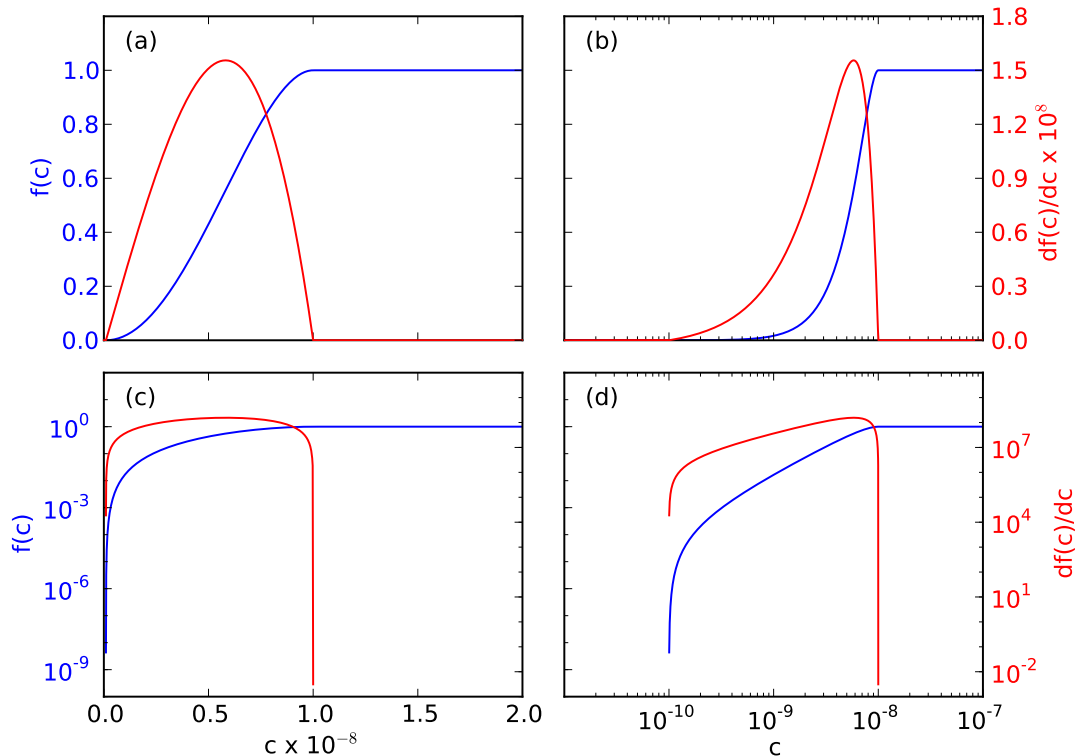


Figure 14. Smoothed cutoff function (Eq. 21) and derivative (Eq. 22). The y axis is in log in (c) and (d), while the x axis is in log in (b) and (d). Even though smoothed, the cutoff is a steep transition. The derivative varies by orders of magnitude in a small concentration range and requires small time step size to march through.

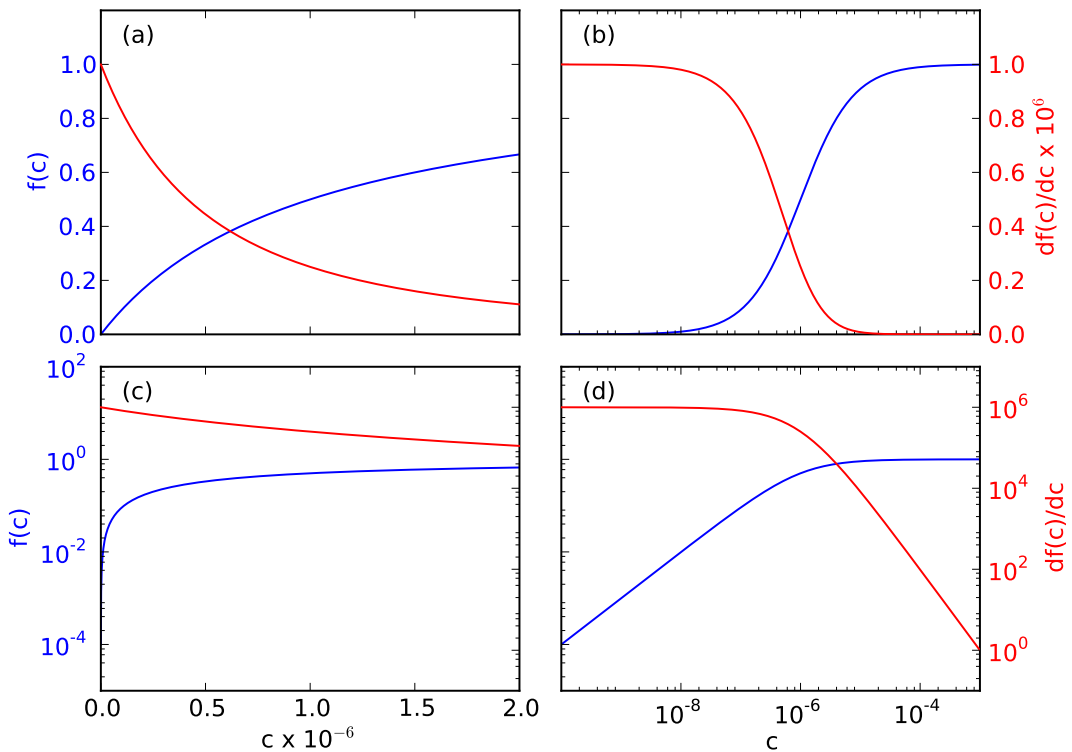


Figure 15. Monod substrate limiting function (Eq. 24) and derivative (Eq. 25). The y axis is in log in (c) and (d), while the x axis is in log in (b) and (d). As the function switches from zero-order to first-order, the derivative jumps six (k_m^{-1}) orders of magnitudes, requiring small time step size to step through.

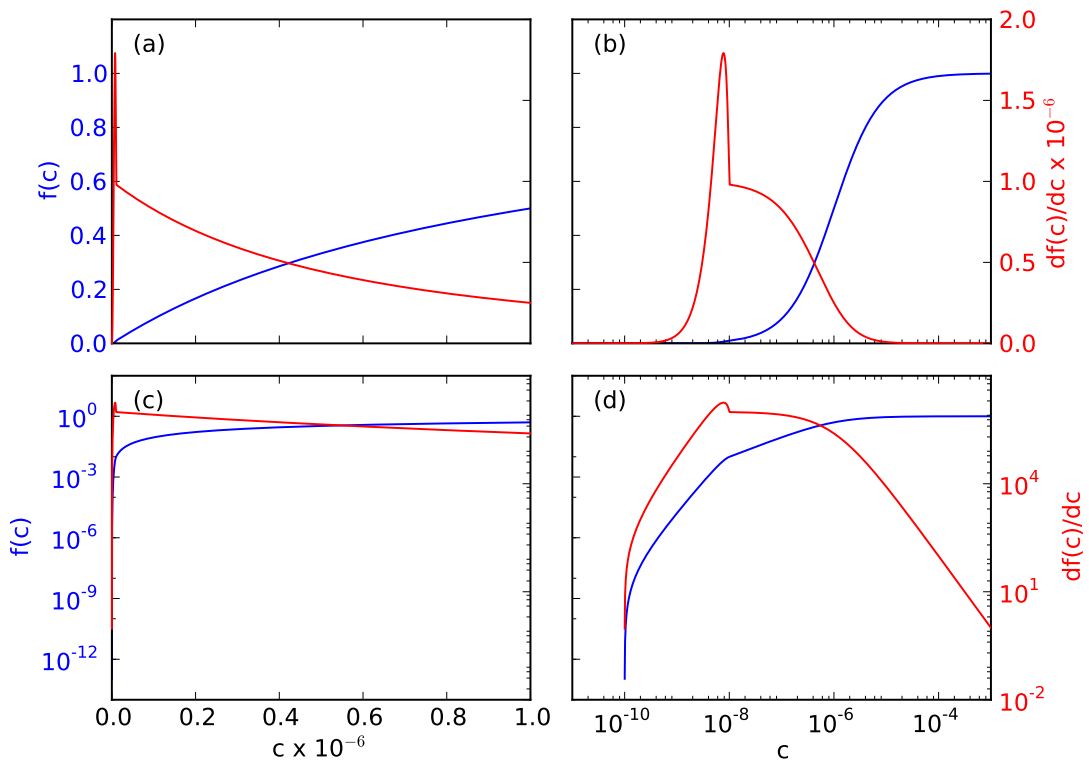


Figure 16. A combination of the Monod substrate limiting function (Eqs. 24 and 25, Fig. 15) and the smoothed cutoff function (Eqs. 21 and 22, Fig. 14) introduces steep transitions that require small time step sizes to march through.